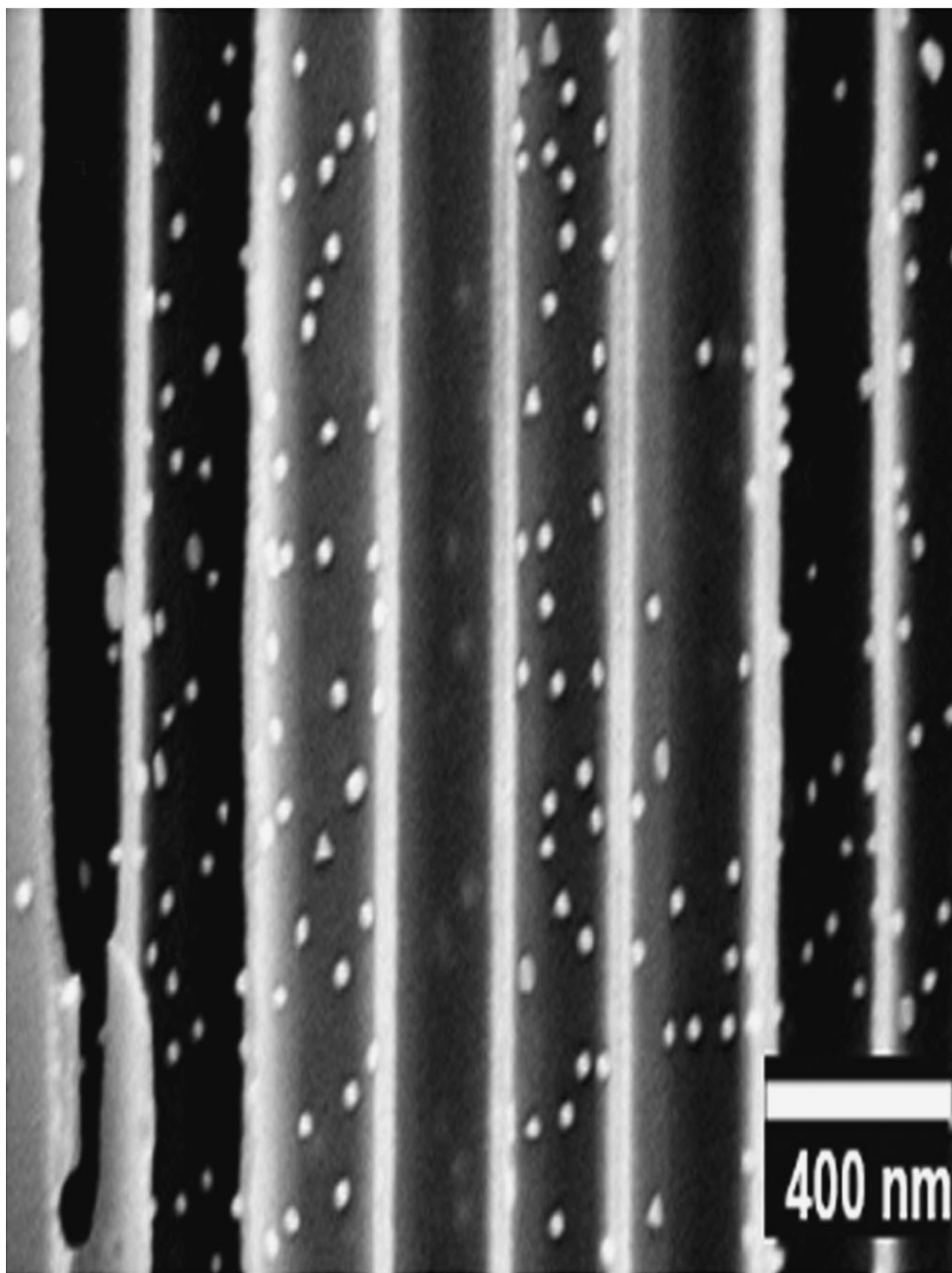


DOI: 10.1002/sml.200800337

Nanostructured Surfaces and Assemblies as SERS Media

Hyunhyub Ko, Srikanth Singamaneni, and Vladimir V. Tsukruk*



Cross-sectional SEM image of porous alumina membranes decorated with Au nanoparticles

From the Contents

1. Introduction..... 1577
2. Electromagnetic Enhancement and Nanostructures... 1580
3. Highly Ordered 1D, 2D, and 3D Metallic Nanostructures... 1585
4. Practical Applications of SERS-Active Nanostructures... 1593
5. Conclusions 1595

Keywords:

- metallic nanostructures
- surface-enhanced Raman scattering
- surface plasmons

NANO MICRO
small

Metallic nanostructures attract much interest as an efficient media for surface-enhanced Raman scattering (SERS). Significant progress has been made on the synthesis of metal nanoparticles with various shapes, composition, and controlled plasmonic properties, all critical for an efficient SERS response. For practical applications, efficient strategies of assembling metal nanoparticles into organized nanostructures are paramount for the fabrication of reproducible, stable, and highly active SERS substrates. Recent progress in the synthesis of novel plasmonic nanoparticles, fabrication of highly ordered one-, two-, and three-dimensional SERS substrates, and some applications of corresponding SERS effects are discussed.

1. Introduction

Inelastic light scattering by a molecule with the quantized vibrational signature is the physical phenomenon behind Raman spectroscopy.^[1] Despite the rich information offered by regular Raman spectroscopy, it has not been the primary choice as a handy analytical tool comparable to Fourier-transform infrared (FTIR) or UV/Vis spectroscopy due to the inherent limitation, “feeble signal”. The weak signal is due to the extremely small Raman scattering cross section for most molecules except some special cases of resonating molecular structures. For example, the benzene molecule, which is a relatively strong Raman scatterer,^[2,3] exhibits a scattering cross section of $2.8 \times 10^{-29} \text{ cm}^2 \text{ molecule}^{-1} \text{ sr}^{-1}$, which is 12–14 orders of magnitude lower than typical fluorescence cross sections.

The discovery of surface-enhanced Raman scattering (SERS) nearly 30 years ago opened a new avenue for Raman spectroscopy by creating excitement in the scientific community.^[3–5] The dramatic enhancement of the intensity of the vibrational spectra from the analyte adsorbed on a rough (at the nanoscale) metal surface, which seems to be simple for experimental realization, was intensely investigated to understand the underlying physical phenomenon responsible for the effect (for a general overview of theories, see References [6–10]). Figure 1 shows the number of publications over the past 30 years in this field, demonstrating a dramatic increase in the research activity, especially in the past 4–5 years. This spark is due to numerous factors of a technical nature (single-molecule detection, nanotechnology advancement, improved instrumentation capabilities) as well as societal old and novel needs (health care, safety, terrorist threats; see the recent Chemical Reviews issue on chemical sensing, particularly, References [11,12]).

The key impediment for the practical use of SERS-based sensors is the lack of robust and facile fabrication strategies for reproducible SERS substrates with large and stable Raman enhancement. Even though traditional SERS substrates, such as electrochemically roughened metallic surfaces, colloidal metal nanoparticles, metal islands, and fractal films, can provide significant SERS enhancement (for reviews, see References [13–15]), the highly ordered SERS substrates with reproducible and deterministic geometries with much higher Raman enhancement are needed for routine measurement of trace-level analytes. With the help of modern nanotechnology to control nanoscale structures and materials, much progress has been recently made.

The discussion of such highly ordered metallic nanostructures is the subject of this Review. We will briefly describe the mechanistic aspects of SERS from an electromagnetic enhancement standpoint and focus on the design, synthesis, and assembly of nanostructures for enhanced Raman scattering. We will discuss recent progress on the fabrication of SERS substrates with ordered one-dimensional (1D), 2D, and 3D nanostructures, especially metallic nanostructures showing a variety of intriguing surface plasmonic properties and corresponding SERS effects.

1.1. Electromagnetic and Chemical SERS Enhancement

It is important to note that after much debate, it is currently widely accepted that the SERS can be discussed in terms of electromagnetic and chemical enhancements, in which the former term is responsible for the major portion of SERS enhancement.

Electromagnetic enhancement is caused by the excitation of collective oscillations of the conduction electrons in a metal nanoparticle (surface plasmons; see Scheme 1).^[16] Excitation of the surface plasmon results in the enhancement of the local field experienced by a molecule adsorbed on the surface of the nanoparticle. Although the increase in the local electric field is usually modest, the enhancement in the inelastically scattered light intensity scales to the fourth power, causing a remarkable SERS effect. However, the enhancement effects are highly localized and decay rapidly as the separation between the analyte and the metal particles increases, making SERS a

[*] Dr. H. Ko,⁺ S. Singamaneni, Prof. V. V. Tsukruk
School of Materials Science and Engineering and
School of Polymer, Textile, and Fiber Engineering
Georgia Institute of Technology, Atlanta, GA 30332 (USA)
E-mail: vladimir@mse.gatech.edu

[+] Present address:
Department of Electrical Engineering and Computer Sciences
University of California at Berkeley, Berkeley, CA 94720 (USA)

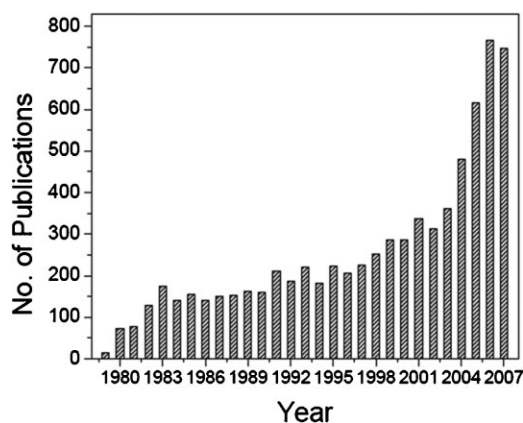
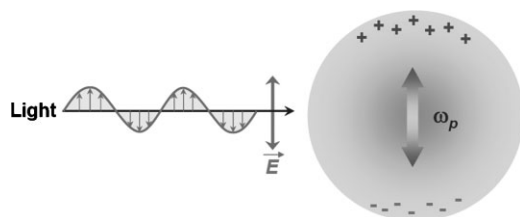


Figure 1. The number of annual publications obtained from SCI FINDER with keyword “SERS.”

truly surface-sensitive technique.^[17] The size of the metal nanostructures for the excitation of the surface plasmons have an upper bound as the wavelength of the excitation light to ensure dipolar excitations since higher-order multipole excitations are not favorable for Raman excitations. However, it is important to note that the higher-order multipole excitations contribute significantly to the electromagnetic enhancement for particles separated by distances smaller than their diameter.^[18]

Chemical effect is another independent mechanism that enhances the Raman-scattering cross section of the analyte adsorbed on the metal surface.^[19] The rationale behind the prediction of this secondary, independent, and relatively weak enhancement is the dependence of the enhancement on the chemical nature of the analyte molecule or structure. Whereas electromagnetic enhancement is a chemically non-selective mechanism, more than two orders of difference in the enhancement can be observed between, for example, CO and N₂ molecules, due only to the chemical-enhancement mechanism.^[20] The electronic states of the analyte molecule are either shifted or broadened due to either the interaction with metal or the origin of new electronic states, resulting in additional enhancement often termed as chemical enhancement. The proximity between the metal and the analyte molecules adsorbed on the surface causes electronic coupling by a charge-transfer mechanism, resulting in resonant intermediate states and thereby enhancing Raman scattering.^[21] One of the most popular examples of resonance Raman



Scheme 1. Schematic image of plasmon oscillation for a metal nanoparticle. Interaction of the electromagnetic wave with a metal causes the free electrons to coherently oscillate at the plasmon frequency (ω_p) against the immobile positive-ion lattice.



Hyunhyub Ko received his Ph.D. in Materials Science and Engineering from Georgia Institute of Technology in 2008, M.S. in Materials Science and Engineering from Iowa State University in 2004, M.S. in Chemical Engineering from Yonsei University in 2001, and B.S. in Chemical Engineering from Chung-Ang University in 1999. He is currently a postdoctoral researcher at the University of California,

Berkeley. His research interests are in the area of directed assembly of nanoscale materials and their applications in sensors and electronic devices.



Srikanth Singamaneni received his M.S. degree in Electrical Engineering from Western Michigan University in 2004 and is currently pursuing his Ph.D. in Polymer Materials Science and Engineering at Georgia Institute of Technology. He has co-authored more than 30 refereed articles in archival journals and made presentations at national conferences. He is a recipient of the Best-Poster Award

at the Materials Research Society National Meeting, Spring 2007. His current scientific interests include the interaction of electromagnetic radiation with metal nanostructures, SERS trace chemical and biological detection, and fabrication of nanostructured materials for physical and chemical sensors.



Vladimir V. Tsukruk received his M.S. degree in Physics from the National University of Ukraine, Ph.D. and D.Sc. in Chemistry from the National Academy of Sciences of Ukraine, and completed post-doctoral positions at U. Marburg and U. Akron. Currently, he is a Professor at the School of Materials Science and Engineering and School of Polymer, Fiber, and Textile Engineering, Georgia Institute of Technology.

He has co-authored more than 250 refereed articles, 20 invited reviews, and 4 books. His research in the fields of surfaces, interfaces, molecular assembly, nano- and bio-inspired materials is honored by the NSF Special Creativity Award (2006), NSF RIA Young Investigator Award (1994), and Humboldt Fellowship (1990), among others. He serves on the editorial advisory boards of *Polymer* and *Current Chemical Biology* and has supervised more than 30 graduate students and postdocs.

scattering that is widely exploited is that observed for carbon nanotubes (not discussed here).^[22–24]

In most cases, both electromagnetic and chemical contributions exist simultaneously, in which the former can give up to 10^{12} enhancement while the latter is considered to be usually in the range of 10–100.^[25] The 10^{12} electromagnetic enhancement factor is typically reported in the case of single-molecule experiments. However, it is worth noting that in a recent report the enhancement factors described for single-molecule detection have been overestimated by four to five orders of magnitude owing to various factors.^[26]

While there is a consensus regarding the existence and nature of chemical enhancement, the magnitude of the enhancement remains unclear. For instance, recent experimental observations and theoretical estimates suggest possible contributions from chemical enhancement as high as 10^5 – 10^7 .^[27–29]

1.2. SERS Experiments and Enhancement Phenomenon

SERS experiments can be broadly classified into two categories, namely, “average SERS” and “single-molecule SERS.” In the average SERS experiment, the spectra obtained are ensemble averages of the signal from a relatively high concentration of the analyte adsorbed on the nanostructures. At this length scale, moderate enhancements (10^5 – 10^8) have been achieved for a wide variety of nanostructures. The technique is usually adapted for reliable quantitative analysis of the analyte under detection. From an experimental viewpoint, it is desirable to improve the enhancement factors by proper design and assembly of the metal nanostructures on the substrate.

In sharp contrast, single-molecule SERS involves detection of the signal from ultralow concentration of the analyte molecules (in theory and some experiments, down to a single molecule) present at a hot spot with enhancement factor claimed (usually based upon simple estimations of analyte molecule concentration) to be as high as 10^{14} . It is a well-accepted rule-of-thumb that the higher the enhancement of Raman cross-section, the more localized are the zones of high Raman activity.^[30]

The detection of the single molecule rejuvenated interest in the phenomenon of SERS and brought the technique on par with fluorescence and frequency-modulated optical absorption. One of the main features of the single-molecule SERS response, markedly different from the average SERS effect, is the so-called blinking of the signal, where the observed position, bandwidth, and the intensity of the normal Raman modes exhibit fast temporal fluctuations.^[31] While the name “blinking” suggests a phenomenon normally related to the fluorescence, the origin of the phenomenon in SERS is still under debate.

As mentioned above, the SERS effect is the product of the individual contributions from electromagnetic and chemical enhancements. Traditionally, the SERS enhancement factor has been estimated by a simple comparison of the enhanced Raman signal with the normal Raman signal obtained under identical experimental conditions. This technique is accept-

able for average SERS experiments, where the enhancement of the relatively uniform SERS substrate is compared with the similar substrate. However, apart from the inherent assumptions that all the experimental conditions remain exactly the same for SERS and normal Raman, one of the primary drawbacks of the technique is the assumption that nearly all the molecules contribute to the observed SERS signal. This assumption causes the common underestimation of the enhancement factor.

An alternate method was introduced in mid-1990s where the enhancement of the vibrational cross section is estimated from the relative magnitude of Stokes and anti-Stokes Raman modes.^[32,33] The vibrational pumping causes a deviation in the anti-Stokes-to-Stokes ratio different from that of the normal scattering process, which is governed by the Boltzmann distribution. For large surface enhancement, the enhanced cross section plays a significant role in the population of the anti-Stokes, given by $P_{\text{as}}^{\text{SERS}} = \left(N_0 \exp\left(-\frac{h\nu_m}{KT}\right) + N_0 \sigma^{\text{SERS}} \tau_1 n_L \right) \sigma^{\text{SERS}} n_L$, where N_0 is the number of molecules in the vibrational ground state, n_L the laser intensity, σ^{SERS} is the effective SERS cross section, τ_1 the lifetime of the first excited vibrational state, T the sample temperature, and h and K are Planck's and Boltzmann's constants, respectively. The first term of the equation corresponds to the anti-Stokes band due to thermal contributions (same as the normal Raman). However, the second term, which is negligible for normal Raman process, dramatically increases and becomes comparable to the thermal contribution for high enhancement. This change can be used to estimate the effective SERS cross section of the analyte molecule, although this method is truly reliable only for very strong enhancement.^[32]

1.3. Theoretical Estimation of SERS Enhancement

The need to develop new theories to corroborate the experimental observations and to design experiments with great precision has become more important with the advent of nanostructured materials with complex shapes, multilength-scale spatial distributions, and variable dielectric ambient. Various computational models, such as discrete dipole approximation (DDA),^[34] the multipole–multipole method,^[35] the time-domain finite-element method,^[36] and the modified long-wavelength approximation^[37] have been employed to calculate the optical properties (such as electromagnetic enhancement and extinction) of various metal nanostructures.

Among recent developments is a noteworthy study by Hao and Schatz, who performed a series of theoretical calculations of the electromagnetic field in proximity to individual and dimer metal nanospheres and prisms using DDA.^[38] From the simulation results, they have concluded that dimer nanoparticles separated by 2 nm exhibited $|E|^2$ values close to 10^5 . In another study, finite-element calculations based on Maxwell equations have also been employed to map the electromagnetic field in the vicinity of the atomic force microscopy (AFM) tip surface.^[39] These simulations provided valuable insight into the tip-enhanced Raman scattering (TERS) mechanism, elucidating that the tip apex angle has a minimum impact on the enhancement. Notingher and Elfick have reported a Raman scattering enhancement of 10^8 for AFM tips

and analyte molecules adsorbed on gold surface when excited with light in resonance.^[40]

It has also been predicted that the enhancement rapidly increases when the wavelength of light is in proximity to the resonance frequency. Although far from experimental realization, Garcia-Vidal et al. have suggested the idea of using silver-filled carbon nanotubes as spectroscopic enhancers and analyzed the enhancement effect from a theoretical point of view.^[41] It has been concluded that the array of metal-filled carbon nanotubes can cause Raman scattering enhancements up to 10^6 for molecules adsorbed on them.

2. Electromagnetic Enhancement and Nanostructures

2.1. Surface Plasmons in Metal Nanostructures

While there are several aspects that affect the magnitude of the SERS enhancement factor, the characteristics of metal nanostructures responsible for the enhanced electric field in close (nanometer) proximity is paramount. In this section, we will briefly review fundamentals of the synthesis of metal nanostructures designed for SERS experiments followed by the discussion of complex nanostructures. Special emphasis will be laid on the correlation between the size, shape, and composition of the metal nanoparticles, their optical properties, and finally on the potential SERS ability.

From an electromagnetic viewpoint, metals can be considered as a plasma of electrons composed of polarizable, free electrons (mobile), and a positive ion core (immobile).^[42] Interaction of the electromagnetic wave with a metal causes the free electrons to coherently oscillate at the plasmon frequency (ω_p) against the immobile positive ion lattice (Scheme 1).^[43] When the electrons are confined in a finite system, say a nanoparticle, where the surface effects dominate the bulk contribution, the plasmon resonance frequency is altered compared to the bulk metal. For example, the plasmon resonance frequency of the spherical metal nanoparticle in vacuum is given by $\frac{\omega_p}{\sqrt{3}}$, where ω_p is the plasmon resonance of the bulk metal in vacuum. The polarization of the electrons in the nanoparticle (with a radius much smaller than the wavelength of the light) by the electromagnetic radiation results in a strong induced electric field at the surface. The field induced at the surface of the nanoparticle is given by $E_{\text{induced}} = \{[\epsilon_1(\omega) - \epsilon_2]/[\epsilon_1(\omega) + 2\epsilon_2]\} E_{\text{incident}}$, where $\epsilon_1(\omega)$ is the complex dielectric function of the metal structure and ϵ_2 is the relative permittivity of the surrounding medium.

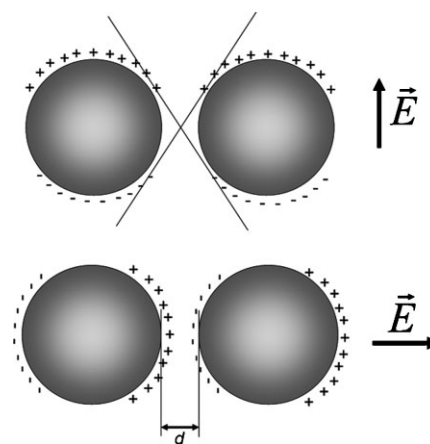
When the exciting electromagnetic radiation is in resonance with the dipolar plasmon of the nanoparticle ($\text{Re}(\epsilon_1) = -2\epsilon_2$), the nanoparticle will radiate light with characteristic parameters for the dipolar plasmon. For three metals, Au, Ag, and Cu, the resonance condition (which depends on the electron density) is met in the visible part of the electromagnetic spectrum, an important property for practical considerations.

The electromagnetic field exhibits a spatial distribution where certain areas are depleted while other areas exhibit an enhanced field. The molecule adsorbed on the surface of the metal nanoparticle is excited by the enhanced field. The increased electromagnetic field results in enhanced Raman

scattered light (E_R) given by $E_R = \alpha_R g E_0$, where α_R is the fraction of the photons undergoing inelastic scattering under normal conditions (given by the appropriate combinations of the components of Raman tensor) and g is the average field enhancement over the particle surface (ratio of the enhanced field to the incident field). Furthermore, the Raman-scattered light is also enhanced by a similar process but to a different magnitude (g') than that of the incident light. Effectively, the average SERS intensity (I_{SERS}) will be proportional to square of the product of both the gains, that is, $I_{\text{SERS}} \propto |gg'|^2$. For low-frequency Raman modes, the gains (g and g') of the incident and Raman-scattered light can be considered to be nearly equal. This feature results in the SERS intensity to be proportional to the *fourth power* of the gain in the electromagnetic field caused by the nanostructure. Hence, even modest enhancement of the electromagnetic field results in gigantic enhancement of SERS cross section.

While the presence of the individual nanoparticles results in the enhancement of the electromagnetic field on the surface, they are seldom reported to exhibit large SERS enhancement. In contrast, the electromagnetic interaction (electromagnetic coupling) between metal nanostructures greatly increases the SERS intensity.^[44–48] In fact, almost all SERS-active systems are composed of *interacting metal nanoparticles* arranged in close proximity to each other. Such an aggregated structured possess a high concentration of the so-called hot spots with enormous local enhancement in the electromagnetic field between nanoparticles for particular polarization direction (coupling effect; Scheme 2).^[49]

The SERS enhancement of the interacting metal nanoparticles exceeds that of the isolated nanoparticles by nearly five to six orders of magnitude.^[14] In a typical SERS experiment, the enhancement is the sum of enhancement sprouting from nanoparticles in various topologies (single



Scheme 2. Schematic image of the reason why light polarized with the E vector along the interparticle axis results in huge enhancements in the gap between the two nanoparticles. For light polarized along the interparticle axis the proximity of the charges (induced by the optical fields) to the molecule can be made arbitrarily small and hence the field sensed by the molecule is commensurately large as the nanoparticles are brought closer together. This capability is not available for light polarized orthogonally to the interparticle axis. Reproduced with permission from Reference [49].

particles, dimers, and multiparticle aggregates). It is important to note that the enhancement obtained from nanoparticle aggregates with narrow interparticle gaps completely dominates over that of any isolated nanoparticles.^[50–52]

The physical reason behind such a gigantic enhancement for aggregated nanoparticles with narrow interparticle gaps can be understood from a simple electrostatic picture. When two nanoparticles separated by a small but finite distance, the incident electromagnetic field (with the electric field along the nanoparticle axis) causes the polarization of the nanoparticles and sets up surface plasmons in both nanoparticles. As the nanoparticles are brought closer, the plasmons of both nanoparticles start interacting with each other and the analyte molecule residing in the gap is subjected to the large capacitive field arising from the opposite charges separated by a small distance (Scheme 2). This interparticle plasmon coupling is extremely important for the intense enhancement of the SERS signal from molecules adsorbed on the nanoparticle junctions, providing the capability for single-molecule detection.^[32,53,54] It should be noted that there has been a significant controversy over the nature of single-molecule SERS but this issue is beyond the scope of our Review.^[55–57]

2.1. Size and Shape of the Metal Nanostructures

The plasmon resonance, electromagnetic-field enhancement, and hence the SERS enhancement critically depend upon the size, size distribution, surface state, surrounding environment, shape, and nature of the metal nanostructures. The metal structures responsible for the SERS effect must be significantly smaller than the wavelength of the exciting electromagnetic radiation. It is clear that SERS-active systems must possess features in the range of 5–100 nm while the strongest SERS effects are usually observed for nanoparticles with a size of 20–70 nm (strongly dependent upon shape, materials, environment, and excitation wavelength). On the other hand, the size of the nanoparticle cannot be much smaller than 5 nm as the particle starts deviating from the pseudo bulk-plasmon behavior and starts exhibiting quantum effects. In fact, for nanoparticles that are too small, the electronic scattering at the surface plays a major role, resulting in the depletion of the electrical conductivity, leading to poor polarizability of the particle and hence degrading the plasmon resonance quality and SERS enhancement.

The plasmon resonance frequencies of the nanoparticles also depend on their size (with some shift caused by variable environment) and are well tabulated for Au and Ag nanoparticles.^[58] For example, the plasmon band of Ag nanoparticles exists at 406 nm for the size of 22.8 nm while nanoparticles with a 37.8-nm diameter show a peak at 428 nm, a significant red shift.^[59] It is also well known that the electric-field enhancement is maximized when the source frequency is in resonance with the plasmon band maximum.^[60] For instance, Xia and co-workers have performed a systematic study of the SERS enhancement from sharp and truncated Ag nanocubes with a size ranging from 60 to 100 nm.^[61] They have observed higher SERS enhancement for particles of larger size (90 and 100 nm), which is primarily attributed to the overlap between the laser source and plasmon resonance band. In a

similar manner, the optimal length of the silver nanorods with a diameter of 37 nm was found to be 62 nm for highest SERS enhancement when a 632-nm laser was employed as an excitation source.^[62]

An important consideration is the shape and exposed crystal planes of the metal nanostructures. This issue has been recently addressed by Zhang et al., who studied the SERS spectra of rhodamine B at the surface of Ag colloids of three distinct shapes (particles, wires, and plates).^[63] They have concluded that the nanoparticles exhibit better enhancement compared to nanowires, and nanowires are better than nanoplates. Particular crystal facets can cause even more dramatic effects, where planes of higher energy form the edges and corners of the nanostructures and act as hot sites for the enhancement. On the other hand, it was found that silver platelets and silver-coated gold nanorods are most effective for achieving high SERS enhancements.^[64] The SERS sensitivity exhibited a strong correlation with the size and the enhancement diminished for platelets larger than 100 nm. Furthermore, it has also been demonstrated that the optimal aspect ratio for the highest SERS enhancement ranges from 2 to 10.^[64]

It is well known that when a spherical nanoparticle is elongated, the surface plasmon band is split into two components: longitudinal (low frequency) and transverse (high frequency).^[65] In the case of nanoprisms, due to their anisotropic shape, four different plasmon resonances are observed: in-plane dipole, quadrupole, out-of-plane dipole, and quadrupole, as theoretically predicted and experimentally observed. In the case of nanoparticles with sharp corners and edges such as nanoprisms and nanocubes, additional enhancement is observed owing to the optical antenna effect.^[66] For instance, the optical bowtie (tip-to-tip triangles) antennas have been extensively investigated from theoretical and experimental viewpoints.^[67–69]

One of the newest synthetic routes to nanoprisms is the photoinduced conversion of metal nanoparticles.^[70] For example, Ag nanoparticles, upon exposure to visible light (350–700 nm), undergo fragmentation, subsequently forming smaller nanoprisms followed by their growth until all nuclei are consumed. Similarly, a thermal-induced spontaneous transformation of Ag nanoparticles to nanoprisms has been demonstrated.^[71] The nanoparticle solution was refluxed in ambient conditions for 10 h, resulting in the transformation of nanoparticles to nanoprisms, accompanied by alteration of plasmon resonances. One important advantage of the thermal transformation is the preservation of sharp edges of the nanoprisms, as opposed to the light-induced conversion where truncated edges were observed, reducing the enhancement effect. The thermally induced synthesis has been further modified to obtain silver nanoprisms with high control over the thickness, which was unattainable with photoinduced conversion methods.^[72] Jin et al. have shown a bimodal size distribution of Ag nanoprisms where the larger nanoprisms formed due to the edge-selective particle fusion.^[73] Various other techniques such as sonochemical and chemical routes have also been utilized for the synthesis of nanoprisms.^[74–77] Several other methods have been shown for the synthesis of exotic nanostructures such as nanocrescents, nanobars,

nanoplates, nanocubes, and nanorice with unique plasmonic signatures.^[78–82]

In related efforts, Norlander et al. have demonstrated the synthesis of star-shaped gold nanoparticles with a slight alteration to the conventional seed growth of nanorods. They have observed a polarization-dependent light scattering with multiple peaks.^[83,84] For nanoparticles with anisotropic shapes, especially with truncated corners, the polarization of light with respect to the truncated corners plays a significant role. For instance, Xia and co-workers have observed dramatic variation in SERS intensity when the nanocubes were oriented at different angles relative to the polarization of the excitation laser (Figure 2).^[81] SERS spectra of 1–4 benzenedithiol adsorbed on Ag nanocubes oriented in different directions with respect to the polarization showed different intensities. The individual nanocubes with sharp corners were the most active when they were oriented such that a diagonal axis (corner to corner) of the cube was parallel to the polarization of the source. On the other hand, nanocubes oriented with one of their faces parallel to the laser polarization were much less SERS active (Figure 2).

2.3. Distance Dependence of SERS Intensity for Different Scenarios

The other important issue in the SERS effect is the distance dependence of the enhancement effect with respect to either the arrangement of analyte molecules and metal surfaces or mutual arrangement of adjacent metal nanostructures.

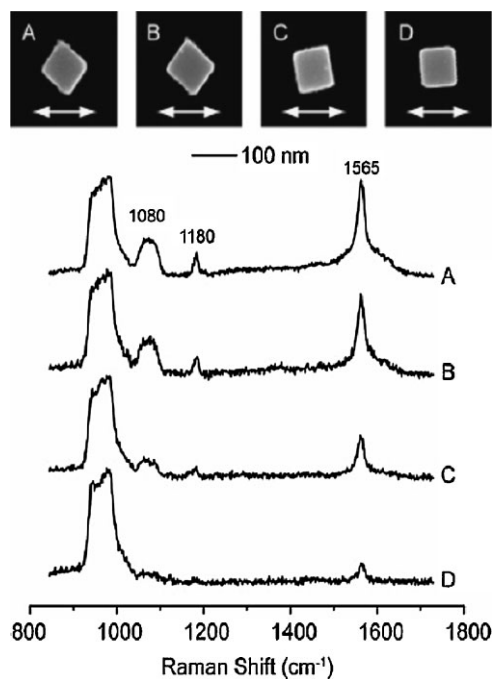


Figure 2. SEM images labeled (A–D) of individual Ag nanocubes. The 100-nm scale bar applies to all images. The white arrows in the images denote the polarization direction of the incident laser. The corresponding SERS spectra from these particles are shown below. Reproduced with permission from Reference [81]. Copyright 2007, American Chemical Society.

While, in the case of the chemical enhancement effect, it is clear that the analyte needs to be chemisorbed to the metal surface for electron transfer to occur, the electromagnetic mechanism needs special consideration. A distance dependence of corresponding intensity, I , has been theoretically predicted in the form $I = (1 + \frac{r}{a})^{-10}$, where a is the average size of the field-enhancing feature and r is the distance of the analyte from the surface of the metal.^[85] However, it is important to note that this effect depends on the fine geometrical features (e.g., shape and mutual orientation) of the nanostructures responsible for the enhancement. Moreover, the coupling of the plasmons in the metal nanoparticle aggregates not only causes the amplification of the polarization thus generating large enhancement but also induces a red-shift of the plasmon resonance peaks as compared to the individual nanoparticle.^[86–89]

There have been several experimental efforts for estimating the distance dependencies. Van Duyne and co-workers have used atomic layer deposition (ALD), which offers a resolution of 0.1 nm, as a spacer layer between the silver film over nanosphere (SERS substrate) and the analyte molecules.^[90,91] Figure 3a shows the series of SERS spectra collected at different thicknesses of the spacer layer. From the

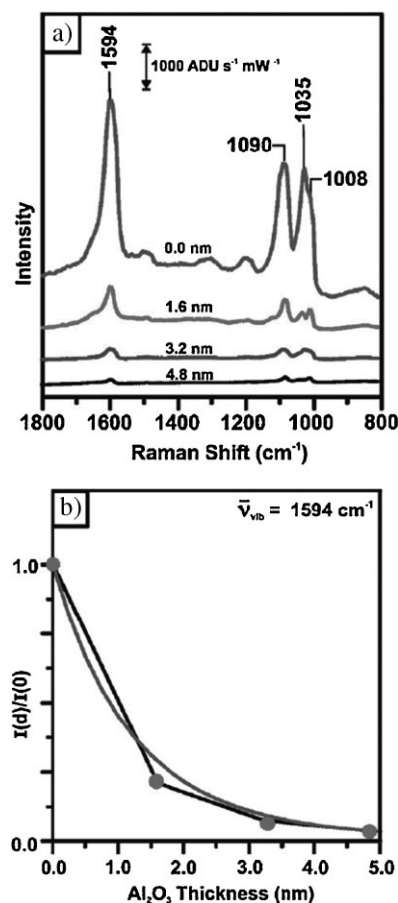


Figure 3. a) SERS spectra of pyridine adsorbed onto silver film covered with alumina (0.0, 1.6, 3.2, and 4.8 nm) at 532-nm wavelength; b) SERS intensity as a function of alumina thickness for the 1594 cm^{-1} band. Reproduced with permission from Reference [90]. Copyright 2006, RSC Publishing.

normalized intensity of the SERS spectra as a function of spacer layer thickness and the fit to theoretical estimation, the authors have estimated that the SERS intensity decreases by a factor of 10 for a spacer layer of 2.8 nm (Figure 3b). In a more recent study, TERS has been employed to probe the distance dependence of the SERS effect. As the tip (metal nanostructure) was retracted from the analyte, a dramatic drop of the intensity was observed within the first 20 nm (signal intensity dropping to one hundredth of the initial intensity). The intensity exhibited a linear drop on a double log scale with further increase in distance.^[92]

In other studies, electron-beam lithography (EBL) has been employed to probe the distance dependence of the plasmonic coupling.^[93–96] Su et al. have demonstrated a near exponential decay of the plasmon shift as a function of the interparticle separation in elliptical gold nanoparticles.^[97] Gunnarsson et al. further confirmed this near-exponential behavior for Ag nanodisk pairs.^[98] More recently, El-Sayed and co-workers conducted a systematic investigation of the plasmon shift of the nanodisk pairs fabricated by EBL (shown in Figure 4a) with varying size and distance.^[99] The experimental observations were analyzed with DDA calculations. They have shown that the plasmon resonances in Au nanodisk pairs exhibited an interparticle plasmon coupling with polarization along the interparticle axis that decays nearly exponentially as given by $y = ae^{-x/\tau}$, where x is the ratio of the gap to diameter of the disk, and τ is the decay constant estimated to be 0.23 ± 0.03 (Figure 4b and c). It is important to emphasize that the decay trend was found to be universal irrespective of the particle size, shape, metal type, and medium dielectric constant. However, the magnitude of the plasmon shift depends on various parameters such as the metal type, medium dielectric constant, and shape of the metal nanoparticles.

2.4. Complex Nanostructures: Dimers, Trimers, Core/Shell, and Bimetallic Nanoparticles

While the EBL technique is an excellent tool for the fabrication of nanostructured arrays with desired geometries, this technique suffers from low throughput and high cost. In view of the large SERS enhancements from dimers and multiparticle aggregates, significant efforts have been made to chemically synthesize dimers and trimers of noble metal nanoparticles. Several methods for the synthesis of controlled gold aggregates and conjugated nanoparticles (dimers) and their use for SERS studies have been recently published. Feldheim and co-workers demonstrated a solution approach, in which they synthesized phenylacetylene-bridged gold dimers and trimers.^[100] Phenylacetylene oligomers were chosen as a basic linker owing to the conformational rigidity and various geometries such as linear, trigonal, and tetrahedral have been tested. In contrast, Huo and co-workers used acid monofunctional gold nanoparticles obtained by a solid-phase synthesis.^[101–103] A similar solid-phase approach also has been undertaken by Sung et al.^[104] Both groups used diamines as a coupling agent in order to obtain dimers of the gold nanoparticles with very small diameters (<2 nm). Wang et al. have developed a polyelectrolyte-based strategy for the synthesis of dimer and trimer aggregates of gold

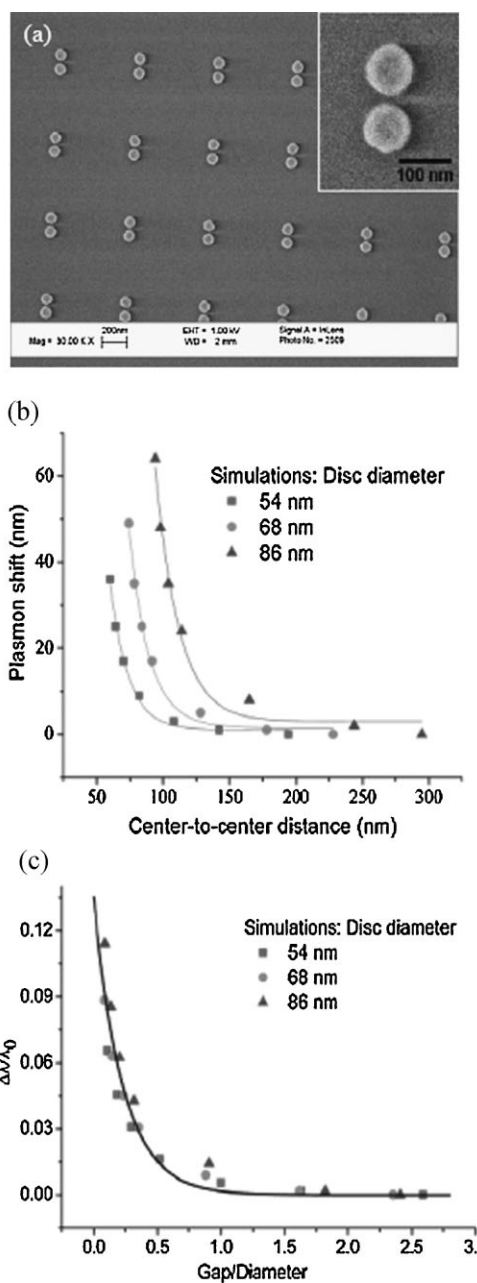


Figure 4. SEM image of nanodisk pairs, having an edge-to-edge separation of 12 nm (inset: a magnified image of a single nanodisk pair). b) Calculated plasmon shift versus the center-to-center distance in Au nanodisk pair for different disk diameters. The solid curves represent least-squares fits to single-exponential decay, $y = y_0 + ae^{(-x/b)}$. c) Calculated fractional plasmon shift versus the ratio of interparticle gap to nanodisk diameter. Reproduced with permission from Reference [99]. Copyright 2007, American Chemical Society.

nanoparticles.^[105] This method is relatively simple and provides gold nanoparticle dimers with larger diameter. Apart from the chemical synthesis of dimers, higher-order systems such as linear chains and multilayered structures can be generated, as will be discussed below.

The ability to obtain enhanced Raman spectra using near-infrared sources is highly desirable owing to the fact that the fluorescence from the analyte is significantly suppressed in this

regime. Furthermore, NIR excitation has been particularly important for biological and biomedical applications of Raman spectroscopy owing to the relative transparency of human tissue in this spectral range. Thus, metal nanostructures with the plasmon resonance extending into infrared regions should be designed for potentially high SERS enhancements with near-infrared sources. While it is possible to tune the plasmon resonance of metal nanostructures by tuning the size, shape, and assembly, these attributes either offer limited tunability before significantly affecting the quality of the resonance or pose extreme challenges in the large-scale synthesis.

Owing to the above consideration, a novel class of nanostructures, metal nanoshells, which offer a wide degree of tunability of the plasmon resonance, have been extensively investigated. In the general case, a metal nanoshell consists of a spherical core enclosed by an ultrathin, conductive, metallic layer.^[106] The electromagnetic-field enhancement, in the case of metal nanoshells, sprouts from strongly interacting plasmons on the inner and outer surfaces of the metallic shell layer.^[107] By varying the composition and dimensions of the shell and the core, the plasmon resonances can be tuned from visible to infrared regions of the spectrum.^[108–110] It is interesting to note that even for a fixed composition, by simply varying the relative dimensions of the core and the shell, the plasmon resonances can be tuned over a wide wavelength range. Zhou et al. pioneered the synthesis of metal nanoshells, in which an Au₂S dielectric core was encapsulated by a gold shell in a single-step process during the mixing of chloroauric acid (HAuCl₄) and sodium sulfide (Na₂S).^[111] By altering the size of the nanoparticles, they demonstrated that it was possible to shift the plasmon resonance to longer wavelengths (≈900 nm) from the conventional plasmon resonance (≈520 nm) of the individual gold nanoparticles.

The primary drawback of the single-step synthetic process is the lack of control over the individual sizes of the core and shell. To overcome this drawback, a two-step process was introduced, which involves the synthesis of the dielectric cores initially, followed by the reduction of the metal on the surface of dielectric cores.^[112] To facilitate metal growth, metal colloids (1–2 nm) are adsorbed onto the core nanoparticles, which serve as the nucleation centers. The technique has been extended to the fabrication of multilayered concentric particles resulting in complex hybridization of plasmon resonances.^[110] The plasmon resonances can be calculated by applying plasmon hybridization theory^[110–114] and the proper geometry can be pre-designed to any frequency in the visible to mid-infrared region.

There are numerous demonstrations in which core/shell nanoparticles have been synthesized and employed for SERS in NIR regions with enhancement as high as 10¹⁰.^[115–118] Silica spheres coated with a gold shell with a varying degree of coverage have been employed for SERS.^[115] When *p*-mercaptoaniline is in solution with gold nanoshells that have their plasmon resonance near 1.06 μm, significant SERS is observed. The strongest Raman enhancement is obtained when enough gold is deposited on the silica cores to form a nearly complete metal shell.^[117]

Bicomponent (bimetallic) nanostructures (typically, combining Au and Ag) are a relatively new class of plasmonic

materials, gaining increased attention in recent years due to synergism of these metals, tunability of plasmon resonance, pre-designed hot spots, and enhanced SERS activity. The bicomponent nanostructures can be primarily classified into three broad categories: core/shell structures, random alloys, and hybrid structures.

Core/shell bimetallic nanoparticles have been synthesized by either segregation during simultaneous reduction or successive reduction of two different metals.^[127,119] Rivas et al. have demonstrated both Au on Ag and Ag on Au structures by citrate reduction.^[120] On the other hand, Srnová-Sýloufová et al. used hydroxylamine to grow Au on Ag seeds.^[121] Core/shell architectures have been achieved in complex shapes such as prisms, wires, and rice to name a few. Bimetallic nanoframes of gold and silver were fabricated by Mirkin et al.^[122] The fabrication involved the synthesis of Ag nanoprisms followed by their conversion into nanoframes and finally backfilling them with Au to form alloyed nanoprisms. Sanedrin et al. have reported seeded growth for the preparation of bimetallic nanoprisms (Au core/Ag shell).^[123] Core/shell bimetallic nanowires have been synthesized and employed to increase SERS enhancement, similar to that designed for spherical nanoparticles.^[124–126]

Alloys of Au and Ag nanoparticles have been synthesized in all possible molar ratios owing to the same crystal structure of the both metals (face-centered cubic (fcc)) and the close lattice constants (4.078 Å for Au and 4.086 Å for Ag).^[127] The alloyed metal nanoparticles have been generally prepared by simultaneous reduction of both the metals.^[128–131] As shown in Figure 5, by varying the molar content of the metals, the plasmon absorption maximum could be tuned from that of pure Ag (≈400 nm) to that of pure Au (≈520 nm). While it is

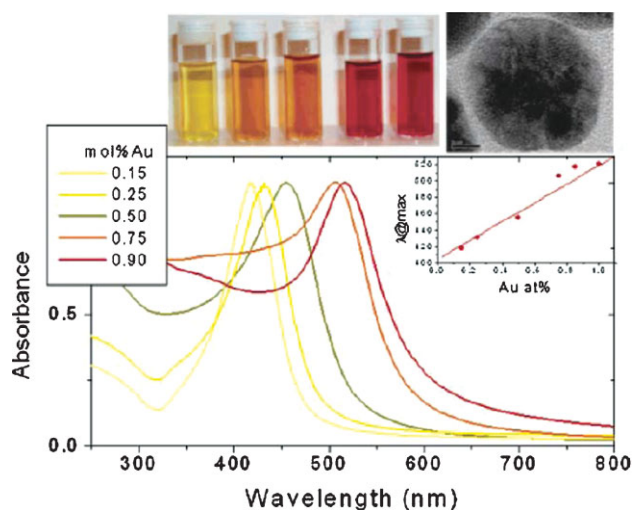


Figure 5. Variation in optical properties (UV/Vis spectra) for Au–Ag alloy nanoparticles with varying composition. The position of the experimental absorption band (dots) is plotted as a function of composition, and the solid line is a linear fit obtained using Mie theory. The high-resolution transmission electron microscopy (HRTEM) image shows the distribution of Au and Ag components within the particles. Reproduced with permission from Reference [127]. Copyright 2006, American Chemical Society.

believed that the alloyed Ag–Au particles are largely homogenous, a surface enrichment with Ag has been recently demonstrated by SERS studies of pyridine adsorbed on the particles.^[132]

Hybrid, organic–inorganic nanostructures are a different class of SERS materials in which two different (composition or shape) component are assembled to form novel structures with a synergistic enhancement in properties. Recently, we have demonstrated bimetallic, silver–polymer–gold, core/double shell nanowires with greatly enhanced SERS ability (Figure 6).^[133] In this design, gold nanoparticles decorate the surface of silver nanowires aided by a three-arm star polymer with functional terminal groups, which act as a linker. Gold nanoparticles form an effective hybrid (polymer–gold) shell of 13-nm thickness with 4-nm gold nanoparticles embedded within the polymer shell around a 65-nm silver core (see the schematic and TEM image in Figure 6a and b).

Figure 6c shows the Raman spectra obtained from the nanocob, silver nanowire, and intersection of two nanowires (see the positions 1, 2, and 3 in Figure 6d and e). Clearly, hybrid silver–gold nanocobs possess significant SERS activity greatly exceeding (by about two orders of magnitude) the SERS enhancement from isolated, bare silver nanowires. Furthermore, it is manifold higher than that at the intersection of two neighboring silver nanowires, which is considered as a traditional hot spot for one-dimensional nanostructures. Figure 6d and e shows the optical image and corresponding confocal Raman mapping, clearly depicting the uniform SERS enhancement for the entire length of the nanocob, as opposed to the bare nanowire, which shows detectable SERS enhancement only at the intersection gap (Figure 6).

3. Highly Ordered 1D, 2D, and 3D Metallic Nanostructures

In this section, we will consider the integration for the design of SERS-active substrates that can include the nanoparticles described above with different nanostructures. We focus on highly ordered 1D, 2D, and 3D SERS substrates (Figure 7). Here, 1D SERS substrates include

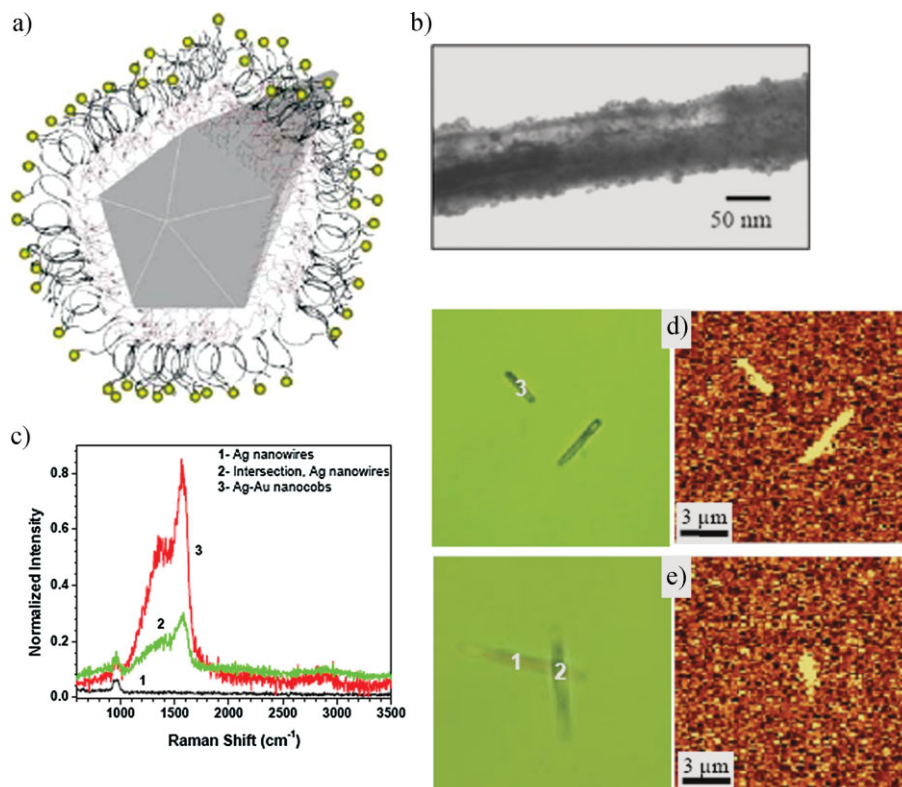


Figure 6. a) Schematic image of silver–gold nanocob. b) TEM image showing the gold nanoparticles decorating the silver nanowires. c) SERS obtained from: individual silver nanowires, intersecting silver nanowires, and silver–gold nanocobs (see corresponding positions 1, 2, and 3 in (d) and (e)). Optical images (left) and confocal Raman mapping (right) of individual nanowires: d) silver–gold nanocobs and e) silver nanowires. The confocal Raman mapping was obtained at 1580 cm^{-1} . Reproduced from Reference [133].

nanoparticle and nanodisk strings. 2D SERS substrates include densely packed nanoparticles and their periodic arrays obtained by, for example, nanosphere lithography. Finally, 3D SERS substrates are open metal nanostructures providing light interaction with the whole structure, such as nanocanal arrays decorated with metal nanoparticles, metallic nanohole arrays, and microhollow optical fibers decorated with metal nanoparticles.

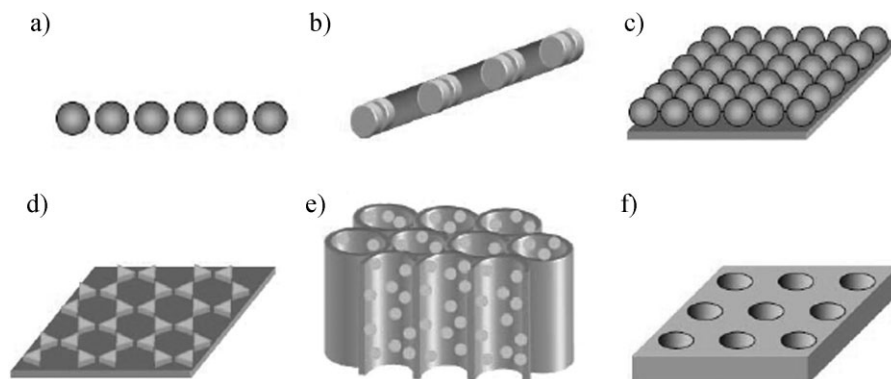


Figure 7. Schematic images of highly ordered 1D, 2D, and 3D SERS substrates. a) 1D metal nanoparticle string, b) 1D metal nanodisk array, c) 2D close-packed nanoparticle array, d) 2D metal nanostructures templated by colloidal crystals, e) nanopore array decorated with metal nanoparticles, f) nanohole array in metal film.

3.1. 1D SERS Substrates

One-dimensional metal nanoparticle arrays with the capability of guiding electromagnetic energy are attractive for nanoscale optical devices and circuits.^[134,135] These nanoparticle arrays can be also excellent candidates for SERS substrates because of the light confinement between nanoparticles, providing enhanced local electromagnetic fields on the junctions of neighboring nanoparticles^[136] and the tunability of localized surface plasmon resonances.^[137–140]

Moreover, recent theoretical studies suggest that 1D nanoparticle arrays are able to combine local field enhancement of nanoparticle dimers with long-range photonic interactions leading to giant field enhancements ($|E|^2 > 10^7$), which enables the detection of single molecules.^[141] The other theoretical report on the self-similar metal nanoparticle chains with progressively decreasing sizes and separations has also suggested the increase in local fields by orders of magnitude due to the cascade effect.^[142]

3.1.1. Solution-Based Assembly of 1D Metal Nanoparticle Arrays

While EBL has been used for the fabrication of 1D metal nanoparticle arrays with well-defined spacing for fundamental study of surface plasmons and subwavelength optics,^[143–145] the fabrication of the massive amount of 1D arrays and assembly of large organized structures will be a key step for practical applications. Several solution-based methods have been reported for the preparation of chain assemblies with interesting surface plasmon properties.^[146] For example, chains of hollow gold nanoparticles have been prepared by templating chains of cobalt nanoparticles assembled by magnetic fields.^[147] In other examples, direct self-assembly of gold nanoparticle strings without using templates has been reported by controlled ligand exchange of citrate ions on the surface of gold with mercaptoethyl alcohol (MEA), a linker molecule between nanoparticles.^[148]

More recently, a solution-based assembly has been demonstrated by using a cationic surfactant, cetyltrimethylammonium bromide (CTAB).^[149,150] In this process, citrate-stabilized Au or Ag nanoparticles were linearly assembled by the addition of appropriate amount of CTAB molecules, which link together the {100} facets of neighboring nanoparticles. Here, the CTAB surfactant has been reported to form bilayer structure on the surface of metal nanoparticles and preferentially bind to the {100} rather than the {111} facets.^[151] As can be seen in Figure 8a, the chain length of 1D Ag arrays can be controlled by adjusting the amount of CTAB,

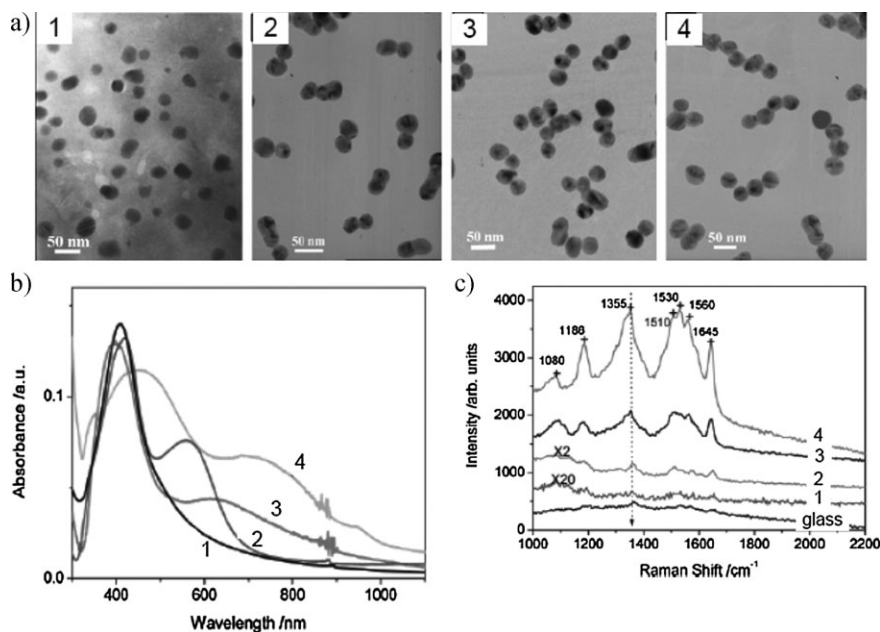


Figure 8. a) TEM images of 1D Ag nanoparticle aggregates: 1) monodisperse Ag colloids, 2) two, 3) three, and 4) four Ag nanoparticle chains. b) Extinction spectra of 1D Ag nanoparticle chains corresponding to samples in (a). c) SERS spectra of 100 mM R6G adsorbed on glass and 5 nm R6G adsorbed on Ag film prepared by self-assembly on PDDA-modified glass with Ag nanoparticle chains 1, 2, 3, and 4 in (a). Reproduced with permission from Reference [150]. Copyright 2007, American Chemical Society.

leading to gradual increase in chain length with the increase in the amount of CTAB. Furthermore, during the growth of 1D nanoparticle arrays, the chain length can be fixed by the addition of 11-mercaptoundecanoic acid (MUA), which prevents further growth of nanoparticle chains by forming carboxylate-terminated protecting layers.

The plasmon resonances of the Ag chain aggregates showed gradual red-shift with increase in CTAB amounts, demonstrating the tunability of the surface plasmon resonance by controlling the length of nanosphere strings (Figure 8b). The SERS spectra of R6G on the monolayer of Ag nanoparticle chain aggregates displayed the increase in the intensity of SERS spectra with increase in the chain length because of an increasing number of interparticle hot spots (Figure 8c). The SERS enhancement factor has been estimated to be about 2.6×10^8 for R6G, which is about two orders of magnitude higher than that of isolated Ag nanoparticles.

3.1.2. Face-to-Face Ordered Nanodisks

One-dimensional, face-to-face nanodisk arrays have been fabricated by on-wire lithography, in which cylindrical nanopores (e.g., porous alumina membranes) have been used for electrochemical synthesis of segmented bimetal nanowires and subsequent wet-chemical etching of one component.^[152] On-wire lithography is an attractive method for preparing 1D SERS substrates because it enables the formation of multiple features with precisely controlled gap (from 5 nm to 8 μ m) and nanodisk thickness (from 20 nm to several micrometers) along the wire.

Recently, Mirkin and co-workers prepared 1D Au nanodisk arrays to investigate electromagnetic enhancement with these structures.^[153] A systematic study of the effects of nanodisk size and interdisk gaps on the SERS intensity was possible due to the ability to precisely control the gap (5–360 nm) and size (360 nm diameter, 40–600 nm thickness) of Au arrays. It was observed that the separation below 30 nm does not significantly affect the SERS enhancement (Figure 9a, d, and g). They also found an optimum thickness (120 nm) of the Au nanodisk, which might be related to the light penetration and confinement within this array (Figure 9b, e, and h). Interestingly, it was observed that there is a non-zero optimum gap size (≈ 30 nm), in contrast to previous suggestions that the maximum SERS enhancement occurs on the junctions with much smaller gaps (<10 nm) (Figure 9c, f, and i). The authors suggested that the decrease in SERS enhancement is due to the excitation of higher multipoles for very small gaps, in which the field enhancements are smaller than that of dipole mode, although it can also be associated with nanoscale roughness of metal surfaces. In a subsequent report, the 1D nanodisk arrays have been proved to be very useful as an encoding system for multiplexed DNA

detection by functionalization with Raman-active chromophores on the spatially separated disk pairs.^[154]

3.2. Two-Dimensional SERS Substrates

In contrast to the disordered metal nanostructures, 2D periodic array of metal nanoparticles have two distinct advantages for SERS applications. The specific surface density of hot spots can be maximized when the nanoparticles are organized in a close-packed manner with the long-range effect providing additional Raman enhancement. The enhancement factors of 2D periodic arrays can be several orders of magnitude higher than those of disordered metal nanoparticle films due to the reduced losses (retardation or damping effects). Theoretical calculations have pointed out that an average SERS enhancement factor of 2D periodic metal nanoparticle arrays with large diameter-spacing ratio (over 30) can approach 2×10^{11} for a Ag nanodisk array and 2×10^9 for a Ag nanosphere array.^[155] The higher SERS enhancement factor for metal nanodisk arrays comparing to those for nanosphere arrays can be ascribed to the electromagnetic-field contribution along the depth for nanodisk arrays.

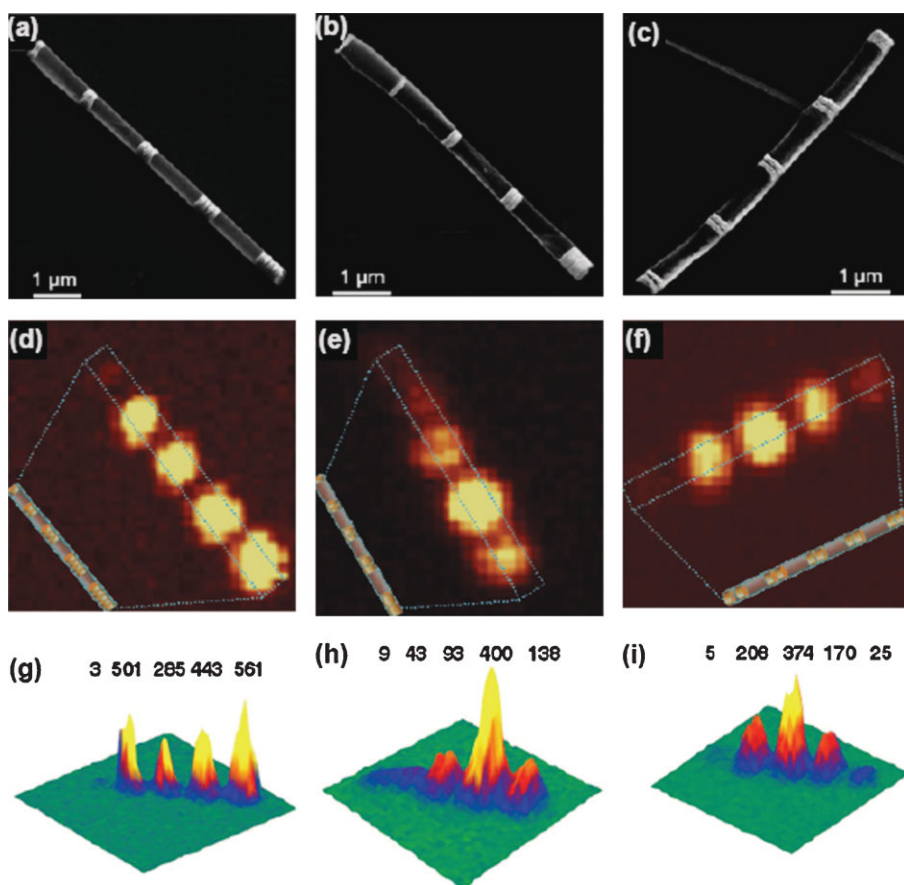


Figure 9. a–c) SEM images of 1D Au nanodisk arrays: a) identical nanodisks with 120-nm thickness and 30-nm separation. b) Identical separations of 30 nm and nanodisk thicknesses of 40, 80, 120, and 200 nm from top left to bottom right, respectively, and at the top left is a single Au disk with 40-nm thickness; c) identical nanodisk thickness of 120 nm and separations of 160, 80, 30, 15, and 5 nm from bottom left to top right, respectively. d–f) 2D and g–i) confocal Raman microscopy images corresponding to 1D Au nanodisk arrays in (a–c) functionalized with methylene blue. Reproduced with permission from Reference [153]. Copyright 2006, National Academy of Sciences.

3.2.1. Close-Packed 2D Metal Nanoparticle Arrays by Self-Assembly

The self-assembly strategy has been one of the most popular methods for the preparation of 2D periodic nanoparticle arrays because of its simple procedure. Simple and well-known strategies can be adopted in generating common 2D plasmonic arrays important for efficient SERS. In this approach, a drop of nanoparticle-containing solution is allowed to evaporate on a properly treated substrate, leading to ordered nanoparticle arrays due to the interplay of capillary and interfacial forces.^[156–158] In comparison to conventional lithographic methods, the great advantage of the self-assembly method for SERS applications is the preparation of extremely narrow interparticle gaps (several nanometers), enabling large electromagnetic-field enhancement. Furthermore, the close-packed structures resulting from self-assembly can provide a maximum surface density of hot spots within an illuminated area.

Most studies with highly ordered 2D metal nanoparticle arrays have focused on the small size of modified nanoparticles (5–15 nm in diameter) because of the relatively easy process

of their assembly. The periodic assembly of larger metal nanoparticles is a challenging task because the long-range capillary forces and van der Waals attractions increase with increasing nanoparticle size, preventing the formation of perfect periodic 2D metal nanoparticle arrays.^[159]

Large-area (over 1 mm²) hexagonal close-packed structures of alkanethiol-stabilized gold nanoparticles have been recently prepared.^[160] The interparticle spacings have been finely tuned from 2.3 to 3.4 nm by controlling the alkyl chain lengths of alkanethiols from 12 to 18 carbon atoms. The surface plasmon resonances of these 2D gold nanoparticle arrays have shown clear interparticle coupling effects with pronounced red-shifting for the decreasing interparticle gaps. In a recent study, hexagonal close-packed structures of silver nanoparticles, prepared by drop evaporation onto a solid substrate, possessed a SERS enhancement factor of 10⁵ for Rhodamine 6G.^[161] However, the optimum size of metal nanoparticles for maximum SERS enhancement was within 30–80 nm.^[64]

The van der Waals attraction can be tuned by using a proper surfactant to assure close packing of larger nanoparticles. For example, a calixarene-based surfactant containing several hydrocarbon tails, which can provide strong repulsive forces, has been successfully employed for the fabrication of highly ordered, close-packed gold nanoparticle arrays by self-assembly of large-diameter gold nanoparticles (up to 170 nm in diameter) at the air/water interface (Figure 10a–c).^[159,162,163] Interestingly, the interparticle spacing decreases from 1 to 0.4 nm with an increase in nanoparticle diameter due to the increased van der Waals attraction. The surface plasmon resonances of the resulting nanoparticle arrays demonstrated significant broadening and red-shift (by several hundreds of nanometers) from the visible to the NIR region (Figure 10d). Such noticeable differences are ascribed to the strong electromagnetic coupling between closely spaced nanoparticles.^[99] It is worth noting that individual nanoparticles show only 47-nm red-shifts and little broadening with increasing diameter from 10 to 100 nm.^[164]

The surface-averaged SERS enhancement factor for these 2D nanoparticle arrays varied from 10⁴ to 10⁷ depending on the size of nanoparticles and the excitation wavelength (Figure 10e).^[163] These enhancement factors are about one to two orders of magnitudes lower than those suggested by theoretical calculations (5 × 10⁸), which can be related to the too small interparticle spacing. It is suggested that while the local field increases with the decrease in spacing, the available field volume decreases as well, restricting the access of analytes.^[155]

CTAB has been successfully used for the assembly of large gold nanoparticles (50-nm diameter) into 2D periodic arrays.^[165] The cationic CTAB surfactant is known to form bilayer structures on the surface of metals, providing positive

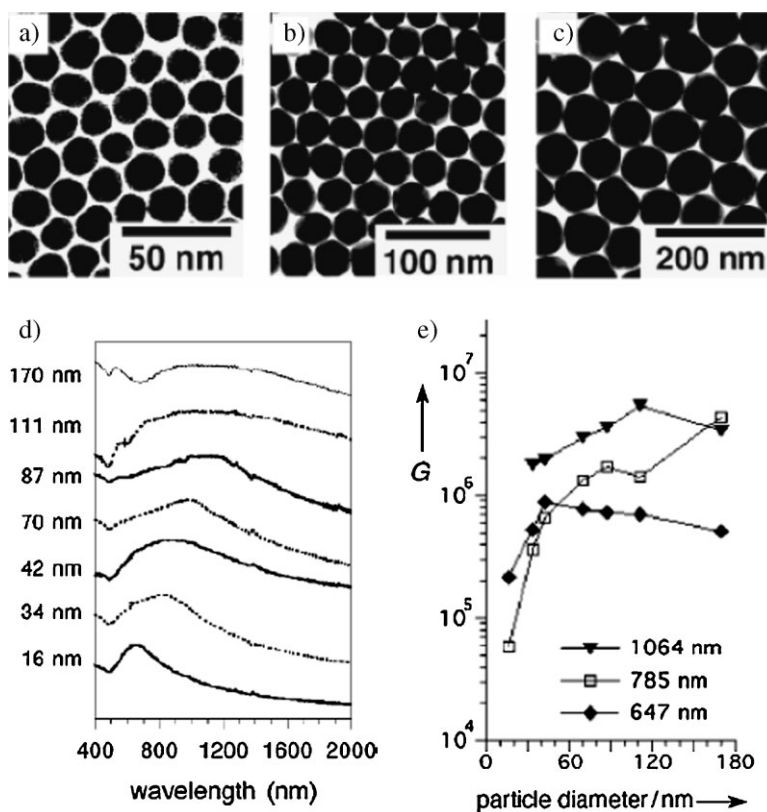


Figure 10. TEM images of 2D close-packed Au nanoparticle arrays with a) 16-, b) 34-, and c) 87-nm particles. d) Extinction spectra of 2D gold nanoparticle arrays with varying nanoparticle sizes. Reproduced with permission from Reference [162]. Copyright 2001, American Chemical Society. e) SERS enhancement factor as a function of nanoparticle diameter and excitation wavelength, based on the characteristic Raman vibration of resorcinarene at 813 cm⁻¹. Reproduced from Reference [163].

charges on the nanoparticle surfaces.^[151] In contrast to the conventional monolayer, the bilayer structure gives rise to the strong repulsive interaction between positively charged nanoparticles, preventing their random aggregation and enabling the dense packing of nanoparticles during solvent evaporation. The interparticle spacing on the resulting 2D nanoparticle arrays was about 8 nm, providing large a SERS enhancement factor of 10⁸ for pMA. The experimental value is close to the theoretical calculation for the perfect Au nanosphere array.^[155] Similarly, 2D nanoshell arrays have been fabricated by assembly of CTAB-stabilized gold nanoshells, providing enhancement of both Raman scattering and infrared absorption on the magnitude of 10⁸–10⁹ for Raman scattering and 10⁴ for infrared absorption.^[166]

3.2.2. 2D Metal Nanoparticle Arrays by Electrostatic Assembly and Langmuir–Blodgett Deposition

The layer-by-layer (LbL) approach is a technique based on alternating electrostatic self-assembly of oppositely charged species to form ultrathin polymer films.^[167–170] LbL assembly has been a powerful tool for the fabrication of organic–inorganic hybrid micro- and nanostructures.^[171–175] With the advantages of well-controlled nanostructures, LbL assembly can be a good platform for 2D metal nanoparticle arrays.

Flexible LbL assembly has been used for the fabrication of free-standing, hybrid metal nanoparticle–polyelectrolyte ultrathin (10–500 nm) films.^[176–181] In particular, the well-controlled intralayer nanoscale thickness has been used to finely tune the plasmon coupling between the intralayer gold nanoparticle arrays in addition to the interlayer plasmon couplings.^[89,182,183]

Langmuir–Blodgett (LB) is a powerful technique to assemble functionalized metal nanoparticles into highly ordered nanostructures.^[184–186] In this technique, a proper colloidal nanoparticle solution is spread onto the water surface and compressed into close-packed arrays by applying surface pressure.^[187,188] The LB technique also provides the ability to tune the interparticle spacing by adjusting the applied pressure.^[184] The ability to tune interparticle spacing and therefore plasmon coupling can provide new capabilities for SERS-based substrates.

Recently, SERS and plasmonic properties have been studied for LB monolayers of silver nanowires,^[189] silver nanospheres,^[190] and non-spherical silver nanoparticles.^[191] The tunable interparticle spacing within Langmuir monolayers has been demonstrated for silver nanocrystals (Figure 11).^[191] As the surface pressure increases, the morphology of the monolayer of silver nanocrystals continuously changes from a hexagonal lattice to a close-packed superlattice at maximum pressure (Figure 11a and c). The color of the nanocrystal film also continuously changes with compression, which immediately indicates the change in coupling between particles along with decreasing interparticle spacing. The evolution of plasmon coupling with increasing surface pressures can be clearly seen in the dark-field scattering spectrum, which shows the appearance of new peaks at the longer wavelengths with an increase in surface pressure (Figure 11d). In another example, the tunable interparticle spacing has been demonstrated by transferring

Ag nanoparticle monolayers prepared by the LB technique onto the temperature-responsive polymer membrane, poly(*N*-isopropylacrylamide) (PNIPAM) followed by the variation of the substrate morphology related to a temperature-controlled response.^[190]

3.2.3. 2D Metal Nanostructures Templated by Colloidal Crystals

Colloidal crystals self-assembled from a monodisperse nanoparticle solution onto a solid surface have been widely used as templates for the fabrication of 2D and 3D periodic nanostructures.^[192] The colloidal crystals provide cheap and facile templated fabrication methods compared to the other lithographic methods because of the easy availability of highly monodisperse colloidal spheres such as silica or polystyrene and the well-developed assembly methods such as drop-casting, spin-coating, dip-coating, and electrophoretic deposition. The typical colloidal crystal possesses hexagonal close-packed morphology at specific facets or where colloidal particles are packed within the monolayer. Well-defined interstitial void spaces between adjacent nanospheres together over large areas provide attractive templates for subsequent fabrication of periodic metallic nanostructures for SERS applications.

For instance, Van Duyne and co-workers introduced a robust and efficient fabrication method for periodic metallic nanostructures, called nanosphere lithography.^[193,194] This method utilizes polystyrene colloidal crystals as physical masks for subsequent evaporation of metal to prepare highly ordered metal triangle arrays (Figure 12). One of great advantages of nanosphere lithography is that the localized surface plasmon resonances of the metallic nanostructures can be easily tuned from visible to the near-IR range because the lateral dimensions of these metallic nanoparticles and interparticle spacing can be precisely controlled by the size of the colloidal spheres and the thickness of deposited metal.

The tunable surface plasmon resonances made it possible to investigate the Raman enhancement by means of UV/Vis absorption spectroscopy, clearly demonstrating that the largest Raman enhancement occurs when the absorption band of metallic nanostructure is located *between the excitation wavelength and the wavelength of Raman-scattered photons*.^[195] These results indicate that the maximum Raman enhancement occurs when the plasmon effect enhances both the incident and scattered photons. Detailed SERS studies on different sets of Ag nanoparticle arrays prepared by nanosphere lithography have demonstrated that enhancement factors of up to $\approx 10^8$ can be achieved for benzene-containing thiols adsorbed on the SERS substrates.^[196] The reader is referred to detailed reviews on nanosphere lithography for SERS applications for further insight.^[197,198]

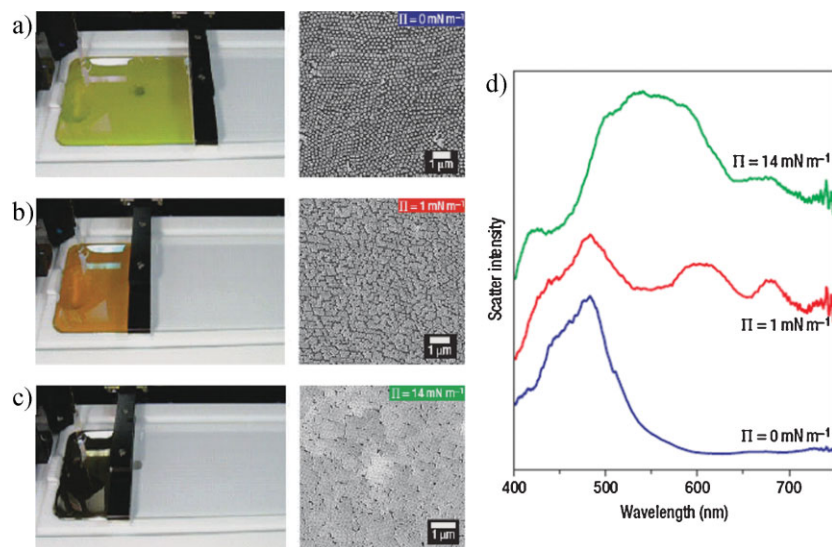


Figure 11. Tunable plasmon response of Ag cuboctahedra superlattice as a function of surface pressure. a–c) Snapshots of the Langmuir films and corresponding SEM images of LB monolayers at different surface pressures. d) Dark-field scattering spectra for the Ag monolayers at various surface pressures. Reproduced with permission from Reference [191] Copyright 2007, Nature Publishing Group.

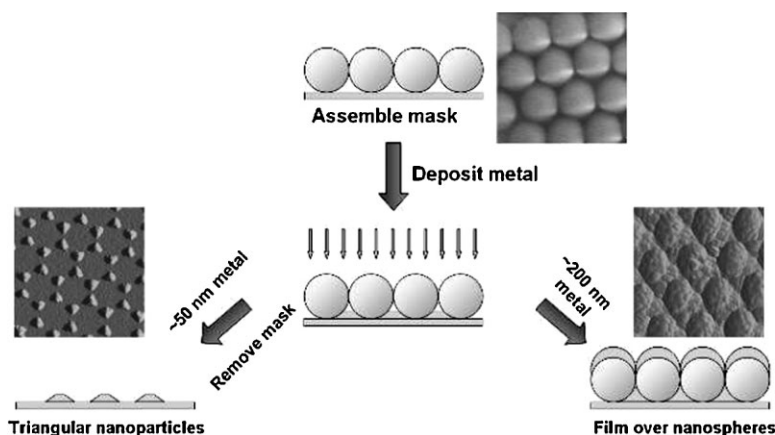


Figure 12. Schematic image of the nanosphere lithography of nanoparticle arrays (left side) and film over nanosphere surfaces (right side) with corresponding SEM images. Reproduced with permission from Reference [198]. Copyright 2006, Materials Research Society.

3.2.4. 2D Nanoporous Arrays

Anodic alumina membranes with highly ordered nanopore arrays have been used as templates to prepare metallic nanostructures for SERS applications.^[199–202] The great advantage of using porous alumina membranes as templates is the capability of precise control of pore size, interparticle distance (i.e., pore wall thickness), and the periodicity of nanopore arrays.

Recently, anodic alumina membranes with hexagonally close-packed nanochannels have been used as templates to fabricate 2D metal nanostructure arrays.^[202] In this report, the interparticle gap has been controllably tuned down to 5 nm by adjusting the periodicity, which enables the systematic study of SERS phenomenon. This study has demonstrated that the SERS decreases exponentially with increase in interparticle spacing due to both the decrease in specific surface density of interparticle gaps located at interfaces and the decrease in local electromagnetic field between nanoparticles. The dependence of Raman intensity on the gap-to-diameter ratio showed an exponential decrease, in accordance with the theoretical prediction discussed above.^[203]

3.3. 3D SERS Substrates

The metal nanoparticle aggregates within colloidal solutions have been the most sensitive SERS systems capable of record limits of detection, down to a single molecule.^[32,53] One of the main reasons for this high sensitivity is the increased light transmission and thus increased light interaction with the mobile nanoparticle aggregates, providing the incoming excitation laser with better chances to meet hot spots. In addition, the sufficiently mobile nanoparticles have better ability to capture analytes within their extremely small gaps. However, when these colloidal nanoparticles are deposited on the planar substrates, the Raman scattering exhibits a dramatic decrease due to the limited light interaction with the ultrathin layer of metallic nanostructures.^[64]

However, the colloidal solution has a limited value for practical applications due to a very limited temporal stability

of dispersed nanoparticle aggregates (frequently, only a few hours or days). The fabrication of *robust 3D metallic nanostructures on solid substrates* with open morphology for efficient light interaction is needed for efficient SERS-active chips. The solid 3D SERS substrates offer large specific surface area for the adsorption of target analytes and provide a large density of hot spots within the laser-illumination area. Moreover, this advantage can be combined with other optical properties related to 3D geometry to assure additional Raman-signal enhancement. Moreover, these solid substrates are usually very stable under ambient conditions.

To limit current discussion, 3D SERS substrates considered in this section do not include, for example, multilayered nanoparticle films with intralayer and interlayer coupling of plasmon resonances, in which the incident-light propagation is limited.^[89] Moreover, while random

nanoporous metallic membranes have been suggested as 3D SERS substrates,^[204,205] we restrict our consideration to only highly ordered 3D metallic nanostructures as SERS substrates with controllable light transmission, which show the highest efficiency.

Most of 3D SERS substrates considered here are fabricated by using 3D templates for the deposition of metallic nanostructures. After their deposition, the 3D templates are frequently removed to generate periodic porous nanostructures. Alternatively, templates can also be included in 3D SERS substrates supporting the metallic nanostructures for improved integrity.

3.3.1. 3D Metal Nanostructures via Colloidal Crystal Templates

While monolayer colloidal crystals have been used as template masks for the fabrication of 2D periodic metal nanoparticles, multilayered colloidal crystals have been widely used for the fabrication of 3D periodic structures of porous metal nanostructures.^[206,207] The deposition of gold nanoparticles in the interstitial spaces of colloidal crystal templates and subsequent removal of these templates give rise to 3D metal nanostructures with long-range hierarchical ordering and nanoscale porosity.^[208] The combination of micro- and nanoporous structures is advantageous for SERS-based sensors due to efficient through transport of analytes and high surface area. Furthermore, the long-range ordering of the periodic metal nanostructures provides additional field enhancement.

For example, in a recent study, Velev and co-workers investigated the SERS properties of 3D gold nanoparticle arrays with a periodic nanoporous structure fabricated by convective assembly of the mixture of polystyrene colloids and gold nanoparticles onto glass substrates.^[209–211] The intensity of Raman scattering of *trans*-1,2-bis(4-pyridyl)ethylene adsorbed on 3D metallic nanostructures prepared by this method was demonstrated to be an order of magnitude higher than that of gold nanoparticle films fabricated without using the periodic colloidal crystal templates.

3.3.2. 3D Vertical Nanopore Arrays Decorated with Metal Nanoparticles

Highly sensitive SERS substrates can be fabricated by depositing metal nanoparticles inside the pores of synthetic nanoporous semiconductors such as silicon^[212] and gallium nitride.^[213] The nanoporous semiconductors are favored as SERS substrates due to their easy fabrication (e.g., by electrochemical etching), uniform pore size, and vertical alignment of the nanopores over large area with precise control of pore depth. However, uniform metal coating deeper into the nanopores is not easily achievable with conventional immersion plating or electrochemical deposition.^[213] To overcome this challenge, thermal decomposition of AgNO_3 solution inside the nanoporous silicon has been used to produce efficient SERS substrates.^[212]

The well-defined 3D nanostructures of anodic aluminum oxide can be also exploited for the fabrication of 3D SERS substrates with metal nanoparticles. Unlike the earlier 3D SERS substrates with limited light propagation, porous alumina membranes with vertical, through nanocanals are beneficial for the efficient light interaction because of optical transparency and waveguide properties.^[214,215]

In fact, we have demonstrated that significant Raman enhancement can be achieved by a 3D porous nanocanal array decorated with gold nanoparticles even without nominal hot spots (Figure 13).^[216] In this case, the fabrication of a 3D SERS substrate is conducted by simply filtrating gold nanoparticles through the PDDA-modified porous alumina membrane. The gold nanoparticles are distributed evenly within nanocanals (Figure 13). For 2,4-dinitrotoluene (2,4-DNT), this nanoparticle-decorated nanocanal array showed about five orders greater enhancement than that of conventional planar nanoparticles array (see Raman spectra in Figure 13). This enhancement cannot be attributed solely to the increase in specific surface area of 3D geometry, suggesting waveguidelike behavior of aluminum oxide nanocanals.

3.3.3. Photonic Crystal Fibers Decorated with Metal Nanoparticles

In fact, as has been demonstrated in recent studies, optical guiding properties can be advantageous for the fabrication of SERS substrates. The porous 3D microstructure of photonic crystal fibers was utilized for SERS detection by decorating metal nanoparticles inside the aperiodic or periodic microscopic hole arrays (Figure 14a).^[217–219] For a typical photonic crystal fiber, the light is guided through the hollow core due to the existence of a photonic bandgap arising from the surrounding air channels. The advantage of using optical fibers is the efficient electromagnetic interaction along the extensive length of the fiber in addition to the large surface area.

Indeed, the decoration of air channels with metal nanoparticles can give rise to an efficient 3D SERS effect (Figure 14b).^[217] As can be seen in Figure 14c, the benzenethiol molecules adsorbed onto the silver nanoparticles within the photonic fiber provide a strong Raman signal, which can not be observed in a control fiber without silver decoration. As compared to the conventional planar SERS substrates or 3D

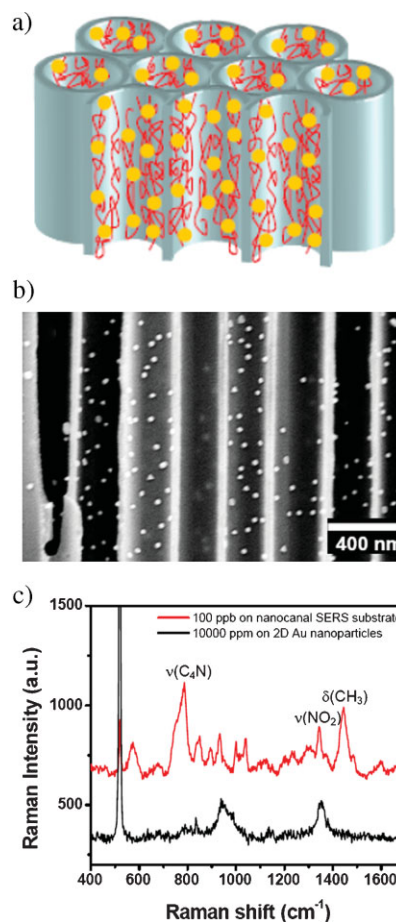


Figure 13. a) 3D nanocanal arrays decorated with gold nanoparticles. Porous alumina membranes are functionalized with PDDA and CTAB-capped gold nanoparticles. b) Cross-sectional SEM image of porous alumina membranes decorated with Au nanoparticles. c) Raman spectra of 100 ppb 2,4-DNT drop-evaporated on the 3D SERS substrate in comparison with 10 000 ppm 2,4-DNT on 2D gold nanoparticle substrate. Reproduced from Reference [216].

SERS substrates without any optical guiding, many more metal nanostructures can be excited by the guided excitation laser traveling along the optical fiber and also the scattered Raman photons can be efficiently collected.

The critical challenge of using optical fibers for SERS detection is the difficulty of filling the hollow fiber with metal nanoparticles without pore clogging. The limited mass transport throughout the continuous microscopic channels calls for the channel diameter to be at least several micrometers. Although the direct capillary suction of liquid colloids into the optical fibers can be applied for the immobilization of metal nanoparticles inside the pores,^[218] the limited filling inside the pores restricts this method to only optical fibers with short length. Recent attempts of using high pressure have shown successful filling of longer fibers with organometallic precursor solution or metal colloids.^[217]

3.3.4. Periodic Nanohole Arrays

Recently, periodic arrays of metallic nanoholes in thin metallic films have attracted much interest due to unexpected

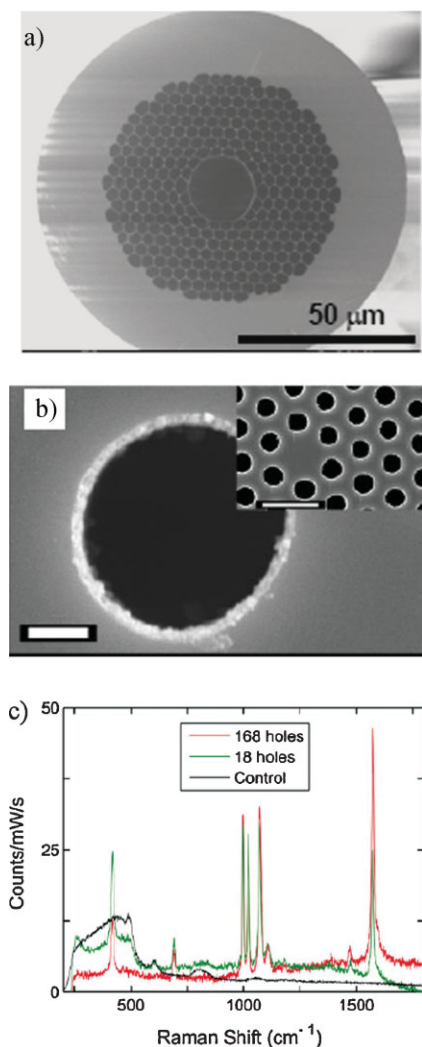


Figure 14. a) SEM image of a photonic crystal fiber with an $\approx 20\text{-}\mu\text{m}$ hollow core and cladding air channel diameter of $\approx 3.5\ \mu\text{m}$. Reproduced with permission from Reference [219]. Copyright 2007, SPIE. b) SEM image of air channel decorated with metal nanoparticles. The inset shows the air-hole arrays with a silica core. c) SERS spectra of benzenethiol adsorbed onto silver nanoparticles within the 18- and 168-hole templates and adsorbed on control optical fiber with no silver filling. Reproduced from Reference [217].

optical phenomena such as extraordinary light transmission and enhanced spectroscopic ability.^[220,221] Metallic nanohole arrays have been demonstrated to enhance fluorescence and IR absorption when the target analytes are adsorbed inside these nanoholes.^[222,223] These arrays are also attractive as surface plasmon resonance substrates due to high sensitivity to the change in refractive index of the dielectric medium.^[224] Central to these phenomena is the excitation of surface plasmon resonances on the surface of metallic nanohole arrays with controlled diameter, spacing, and distribution.

Usually, the subwavelength holes in metal film are fabricated by using focused ion beam (FIB) milling.^[220,222,225] Alternately, nanosphere lithography has been used to fabricate periodic gold nanovoids by electrochemical deposition of Au through self-assembled colloidal crystals.^[226,227] Soft lithography is another powerful tool to fabricate periodic

metallic nanohole arrays over large areas. Odom and co-workers used a poly(dimethylsiloxane) (PDMS) stamp as a phase mask to generate free-standing Au nanohole arrays with high optical quality.^[228,229] The PDMS stamp has also been used in imprint lithography to fabricate periodic Au multi-layered structures consisting of nanohole arrays with a second Au disk layer at the bottom of the holes.^[230]

Nanohole arrays have been demonstrated to exhibit enhanced Raman scattering due to the combined effects of an intense electromagnetic field generated by the surface plasmons and enhanced light transmission.^[231–233] Brolo et al. have demonstrated a SERS enhancement factor of 2×10^5 for resonant analytes when the wavelength of the transmission peak was close to the excitation wavelength.^[231] In a recent study, double-hole arrays in a 100-nm-thick gold film have been fabricated (Figure 15a).^[233] The maximum SERS intensity was observed when the distance between the holes was about 190 nm due to the formation of sharpe

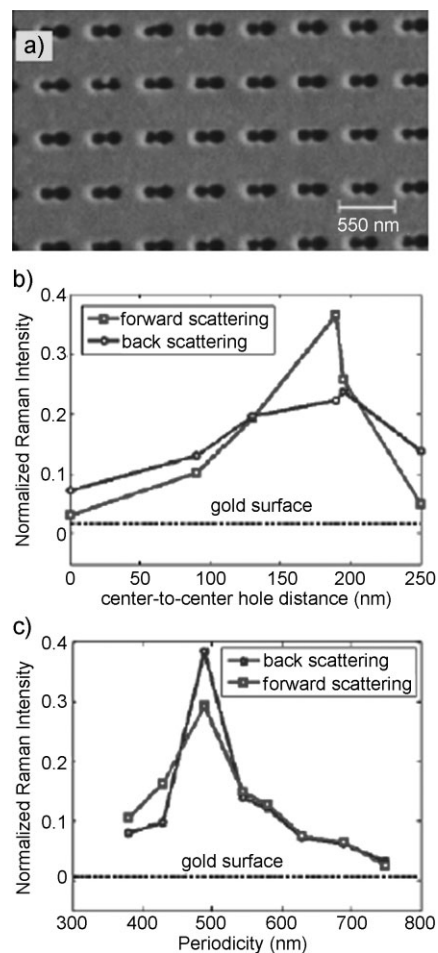


Figure 15. a) Double hole array in gold film with 550-nm periodicity, center-to-center distance of 175 nm, and hole diameter of 180 nm. Normalized SERS intensity in forward- and back-scattering geometries as a function of b) the center-to-center hole distance (for arrays with fixed periodicity at 750 nm) and c) the periodicity (for array with fixed center-to-center hole distance at 175 nm). The intensity of the $591\ \text{cm}^{-1}$ band of oxazine720 is used. The dashed line shows the back-scattering results from the unpatterned surface. Reproduced with permission from Reference [233]. Copyright 2007, American Chemical Society.

apexes (Figure 15b). The SERS enhancement increased about 12 times as compared to that of the nanohole array with non-resonant spacing (Figure 15c).

4. Practical Applications of SERS-Active Nanostructures

Raman spectroscopy has continued to find applications in a variety of fields, which include materials science, biomedical and environmental monitoring, reaction monitoring and industrial processes, chemical sensing, and trace detection.^[234,235] While regular Raman spectroscopy suffices for the most routine measurements, it fails for low quantities of analytes (e.g., self-assembled monolayers (SAMS), ultrathin polymer films, nanomolar analyte solutions), limiting its use as a surface-sensitive technique. Unarguably, SERS has made a significant impact on the field of surface science, imparting single-molecule sensitivity to Raman spectroscopy.

The current and prospective applications of SERS can be classified into two broad categories. The first set of applications involves the technologically important detection of trace amounts of analytes, such as organic compounds, biomolecules, or vapors. In the second set of applications, the technique is employed to monitor physical or chemical processes at the nanoscale. It is worth noting that the vast majority of applied studies reported to date involve simple SERS-active media such as metal colloids with little use of novel nanostructured designs. However, considering significant progress in designing such nanostructures with superior performance, their utilization in practical studies is only a matter of time. Here, we will briefly overview the most recent examples of the aforementioned applications.

4.1. Biological Sensing

Rapid, sensitive, and selective detection of biomolecules is of significant importance in the field of life sciences for health care or therapeutic treatment. While there are several reports where Raman spectroscopy is used as a bioanalytical tool, the application is limited because of the poor sensitivity at clinically important concentrations and physiologically relevant conditions. Moreover, apart from the detection of extremely low concentrations of the biomolecules, it is highly desirable to quantitatively estimate the concentration of the specific analyte. This routine requires extremely reproducible SERS substrates in conjunction with careful calibration.

One example is prostate-specific antigen (PSA), a well-established biomarker for the prostate cancer at ultralow concentrations (a few ng mL^{-1}) in a complex biological fluid. To this end, Grubisha et al. have shown that very low PSA concentration (several pg mL^{-1}) in serum can be detected by binding the specific antibody with bifunctional gold nanoparticles with a monolayer of Raman-active molecules.^[236] Van Duyne and co-workers have demonstrated the quantitative detection of calcium dipicolinate (CaDPA) from bacillus spores, a biomarker for anthrax using silver film over nanosphere (AgFON) substrates. The limit of detection was ≈ 2550 anthrax spores on the AgFON sensor with a data acquisition period of 1 min.^[237] One of the primary drawbacks of the system was the limited long-time stability due to oxidation of the silver.

Overcoming this drawback, the same group later demonstrated simple surface modification to the AgFON by ALD technique.^[237] They coated the AgFON substrates with an ultrathin layer (less than 1 nm) of alumina. The ultrathin alumina layer protected the silver from oxidation yet preserved the electromagnetic enhancement. The resulting substrates enabled a detection limit of 1400 spores and extended (to nearly 9 months) temporal stability. Goodacre and co-workers^[238] have developed a Raman interface to scanning electron microscopy (SEM) for bacterial analysis and have demonstrated identification of SERS-active regions in the matrix through SEM imaging. Several other recent studies report trace analysis of glucose,^[239] gene diagnostics,^[240] and viruses.^[241] While most of the initial studies pertained to in vitro conditions (trace detection and

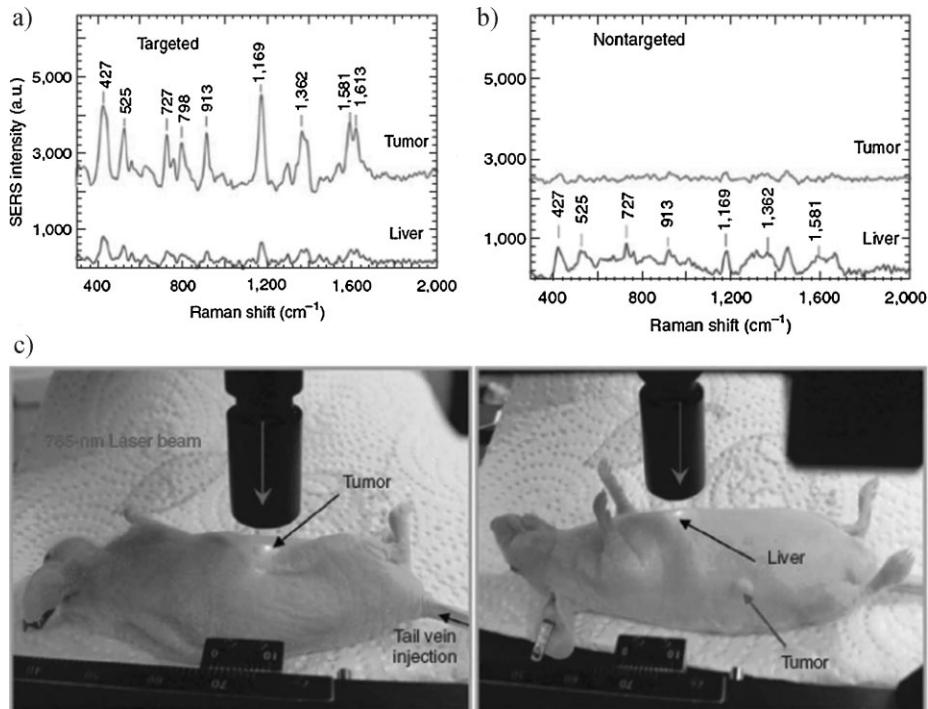


Figure 16. In vivo cancer targeting and SERS detection by antibody conjugated gold nanoparticles that recognize the tumor biomarker. SERS spectra obtained from the tumor and the liver locations by using a) targeted and b) non-targeted nanoparticles. c) Photographs showing the laser beam (785 nm) focusing on the tumor site or on the anatomical location of the liver. The Raman reporter molecule used was malachite green. Reproduced with permission from Reference [243]. Copyright 2008, Nature Publishing Group.

quantitative analysis), in vivo SERS measurements have been recently demonstrated.^[242,243] Van Duyn and co-workers were the first to demonstrate in vivo SERS measurements, in which they subcutaneously implanted functionalized AgFON surfaces into the live rats to quantitatively monitor the concentration of glucose levels in the interstitial fluid.^[242]

An important application of SERS for biological studies is tagging, in which Raman-active molecules are tethered to a nanoparticle or an aggregate exploited for specific biological targets.^[244] Very recently, biocompatible and nontoxic nanoparticles have been applied as SERS tags for in vivo tumor targeting.^[243] Gold nanoparticles have the distinct advantage as SERS tags due to well-established cell-biology methods. However, the functionalization of gold nanoparticles for biocompatibility and for achieving targeted probe delivery is considered to be challenging. Au nanoparticles (63 nm) were tagged with Raman-active markers (1.5×10^4 markers/particle) and were functionalized with poly(ethylene glycol) (PEG) for biocompatibility. Targeted (with specific antibodies and peptides) and non-targeted (accumulation by enhanced permeability and retention) nanoparticles were delivered to mice (Figure 16). The targeted particles exhibited stronger Raman spectra from the tumor sites due to the enhanced accumulation (nearly ten times) compared to the non-targeted particles, as can be seen from the SERS signals obtained from liver (a control for non-specific accumulation) and tumor in the case of the targeted and non-targeted nanoparticles (Figure 16).

4.2. Trace Chemical and Explosives Analysis

The detection of trace-level explosives and hazardous chemicals is in high demand with increasing threat from terrorism and harmful environments.^[245] It is challenging to detect trace-level trinitrotoluene (TNT), one of the most widely used explosives due to its low vapor pressure (≈ 5 ppb). Kneipp et al. were the first to demonstrate the SERS detection of TNT with a detection limit as low as 100 nM (1 pg) level by using colloidal gold and silver.^[246] Dinitrotoluene (DNT), present as impurities in TNT explosives, has also been chosen as a target molecule because it provides higher vapor pressure (100 ppb) than TNT.^[247] Typical detection limits of 0.7–10 pg of 2,4-DNT have been reported with highly oriented silver nanowire films^[189] and rough gold substrates.^[248]

Our group introduced nanocanal arrays decorated with metal nanoparticles as efficient SERS substrates for trace-level detection of DNT.^[216] The minimum detection limit estimated from the signal-to-noise ratio for this spectrum can be as low as 10 fg. The Raman spectrum of 100 ppb 2,4-DNT solution evaporated on a SERS substrate clearly shows NO₂ stretching modes of DNT at 1342 cm⁻¹, distinctive from several PDDA-related Raman peaks such as ν_{C4N} at 783 cm⁻¹ and ρ_{CH3} at 1444 cm⁻¹ (Figure 13c).

4.3. Monitoring Nanoscale Chemical and Biochemical Phenomena

There are numerous reports where SERS has been used to study the nanoscale biochemical phenomena. For instance, SERS has been employed to monitor the release of

neurotransmitter at the single-cell level due to the ability to provide structural information of the released compounds and spatial information about their release sites.^[249] Silver colloids were added to the cell-culture medium, which resulted in the aggregation of the nanoparticles on the cell surface. One of the major advantages of the Raman spectroscopy over IR spectroscopy is the higher lateral resolution in far-field imaging due to the smaller wavelength.

There are numerous examples where SERS has been applied for studying the formation of SAMs on Au and Ag surfaces.^[250,251] In a recent study, Halas and co-workers have reported an interesting carbon-chain-length-dependent surface-enhanced Raman effect for alkanethiol SAMs.^[252] The gold-sulfur bond stretching of the alkane thiol molecules adsorbed on the properly designed Au nanoshells was found to be sensitive to chain length.

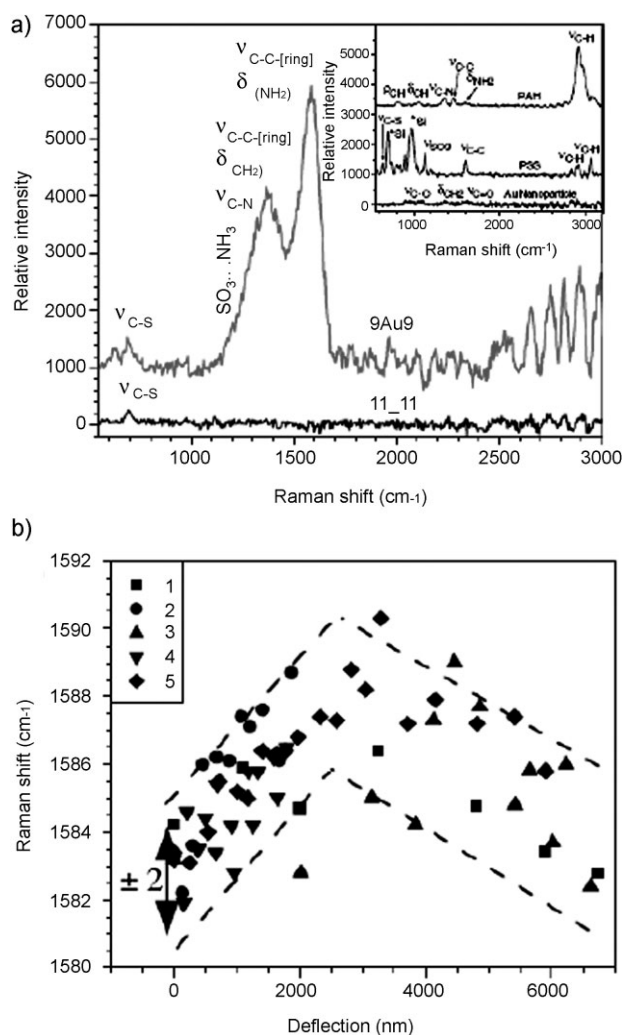


Figure 17. a) Raman spectra of freely suspended nanomembranes showing dramatic enhancement of selected Raman bands after encapsulation of gold nanoparticles. Inset: Raman spectra of bulk materials used for nanomembrane assemblies. b) The peak shift versus nanomembrane deflection for different deformation cycles. Reproduced with permission from Reference [254]. Copyright 2005, American Physical Society.

4.4. Monitoring Micromechanical Behavior

Revealing internal distribution of mechanical stress (e.g., in silicon substrates) is a traditional application of Raman microscopy.^[253] However, for nanoscale structures and for materials with a weak Raman signature, traditional Raman observations should be replaced with a SERS approach.

For instance, in a recent study, SERS has been applied for the in situ monitoring of polymer-chain reorganization in deformed ultrathin, gold-containing LbL films (≈ 60 nm).^[254] LbL films were prepared by sandwiching a monolayer of gold nanoparticles (12.7 nm in diameter) between polyelectrolyte layers. The amount of gold nanoparticles was adjusted to achieve chainlike aggregation with 2–8-nm gaps providing hot spots. For such a design, the strong SERS signals allowed the peak positions and intensity to be monitored in real deformation time, revealing a two-stage mechanism for the stretching of the polymer chains (Figure 17a and b). Under small deformation, a radial reorientation of the side phenyl rings of the polymer backbones was observed while larger deformation resulted in the polymer chains bridging the adjacent nanoparticles.

5. Conclusions

The selectivity and sensitivity (down to single-molecule level) makes SERS one of the most promising analytical techniques for biological, materials, and chemical sciences. With respect to the fabrication of efficient SERS substrates, significant advancements have been made in the synthesis of metal and hybrid nanoparticles with good control over the shape and size. Intriguing optical properties of these nanoparticles in conjunction with their assembly behavior have been extensively studied.

The next critical challenge is the fundamental understanding of the collective optical properties of complex metal nanoparticles when they are assembled into nanostructure arrays and the utilization of these metallic nanostructure arrays for a wide range of applications. Therefore, the development of efficient, robust fabrication strategies of metallic nanostructures with reproducible and well-defined geometry providing giant SERS enhancement represents a key challenges for high-performance SERS-based sensors.

Future efforts should focus on the design of metallic or hybrid structures to precisely control various aspects of related phenomena such as transmission, absorption, scattering, reflection, and propagation of light interacting with the SERS substrate. These nanostructures should be combined with the known hot-spot geometries to efficiently collect and transport the incident and scattered photons along with providing easy access to analytes. In addition to the selected 2D assemblies and novel 3D nanostructures discussed here, a variety of well-known approaches can be exploited to create even more efficient SERS-active nanostructured materials and structures such as complex waveguides,^[215,255] 3D photonic crystals, non-periodic materials,^[256,257] block copolymers with incorporated nanoparticles,^[258] transparent 3D optical resonators,^[259] transparent and porous LbL structures,^[260,261] responsive coatings,^[262] multiplexed soft lithography,^[263] nanofiber

arrays,^[264,265] and free-standing nanocomposites,^[176,178,266] all of which are rarely utilized as SERS-active media in current studies.

Acknowledgements

The authors acknowledge generous support of their work from NSF-DMR, NSF-CBET-NIRT, AFOSR, AFOSR-DURIP, DARPA, DHS, and ARO.

- [1] C. V. Raman, K. S. Krishnan, *Nature* **1928**, 122, 169.
- [2] R. L. McCreery, *Raman Spectroscopy for Chemical Analysis*, John Wiley & Sons, New York **2000**.
- [3] D. L. Jeanmaire, R. P. Van Duyne, *J. Electroanal. Chem.* **1977**, 84, 1–20.
- [4] M. Fleischman, P. J. Hendra, A. J. McQuillan, *Chem. Phys. Lett.* **1974**, 26, 163–166.
- [5] M. G. Albrecht, J. A. Creighton, *J. Am. Chem. Soc.* **1977**, 99, 5215–5217.
- [6] A. Otto, I. Mrozek, H. Grabhorn, W. Akemann, *J. Phys. : Condens. Matter.* **1992**, 4, 1143–1212.
- [7] A. Otto, *J. Raman Spectrosc.* **2002**, 33, 593–598.
- [8] A. Campion, *Ann. Rev. Phys. Chem.* **1985**, 36, 549–572.
- [9] M. Moskovits, *Rev. Mod. Phys.* **1985**, 57, 783–826.
- [10] P. Kambhampati, C. M. Child, M. C. Foster, A. Campion, *J. Chem. Phys.* **1998**, 108, 5013–5026.
- [11] J. Homola, *Chem. Rev.* **2008**, 108, 462–493.
- [12] C. McDonagh, C. S. Burke, D. D. MacCraith, *Chem. Rev.* **2008**, 108, 400–422.
- [13] T. Vo-Dinh, *Trends Anal. Chem.* **1998**, 17, 557–582.
- [14] G. A. Baker, D. S. Moore, *Anal. Bioanal. Chem.* **2005**, 382, 1751.
- [15] V. M. Shalaev, in: *Handbook of Nanostructured Materials and Nanotechnology, Vol. 4, Optical Properties*, (Ed.: H.S. Nalwa), Academic Press, San Diego **1999**.
- [16] A. Knoll, *Ann. Rev. Phys. Chem.* **1998**, 49, 569–638.
- [17] M. Moskovits, D. P. DiLella, K. Maynard, *Langmuir* **1988**, 4, 67–76.
- [18] P. Chu, D. L. Mills, *Phys. Rev. B* **2008**, 77, 045416.
- [19] A. Otto, *J. Raman Spectrosc.* **2005**, 36, 497–509.
- [20] A. Campion, P. Kambhampati, *Chem. Soc. Rev.* **1998**, 27, 241–250.
- [21] K. Kneipp, H. Kneipp, L. Itzkan, R. R. Dasari, M. S. Feld, *Chem. Rev.* **1999**, 99, 2957–2976.
- [22] *Carbon Nanotubes: Synthesis, Structure, Properties, and Applications*, (Eds.: M.S. Dresselhaus, G. Dresselhaus, Ph. Avouris), Springer, New York **2001**.
- [23] S. B. Cronin, A. K. Swan, M. S. Ünlü, B. B. Goldberg, M. S. Dresselhaus, M. Tinkham, *Phys. Rev. Lett.* **2004**, 93, 167401.
- [24] H. Ko, C. Jiang, H. Shulha, V. V. Tsukruk, *Chem. Mater.* **2005**, 17, 2490–2493.
- [25] A. Campion, J. E. Ivanecky, III, C. M. Child, M. C. Foster, *J. Am. Chem. Soc.* **1995**, 117, 11807–11808.
- [26] E. C. Le Ru, E. Blackie, M. Meyer, P. G. Etchegoin, *J. Phys. Chem. C* **2007**, 111, 13794–13803.
- [27] B. Nikoobakht, J. Wang, M. A. El-Sayed, *Chem. Phys. Lett.* **2002**, 366, 17–23.
- [28] D. P. Fromm, A. Sundaramurthy, A. Kinkhabwala, P. J. Schuck, G. S. Kino, W. E. Moerner, *J. Chem. Phys.* **2006**, 124, 061101.
- [29] L. L. Zhao, L. Jensen, G. C. Schatz, *Nano Lett.* **2006**, 6, 1229–1234.
- [30] A. Kudelski, B. Pettinger, *Chem. Phys. Lett.* **2004**, 383, 76–79.
- [31] M. L. Jacobson, K. L. Rowlen, *Chem. Phys. Lett.* **2005**, 401, 52–57.

- [32] K. Kneipp, Y. Wang, H. Kneipp, I. Itzkan, R. R. Dasari, M. S. Feld, *Phys. Rev. Lett.* **1996**, *76*, 2444–2448.
- [33] K. Kneipp, H. Kneipp, P. Corio, S. D. M. Brown, K. Shafer, J. Motz, L. T. Perelman, E. B. Hanlon, A. Marucci, G. Dresselhaus, M. S. Dresselhaus, *Phys. Rev. Lett.* **2000**, *84*, 3470.
- [34] W. H. Yang, G. C. Scahtz, R. P. Van Duyne, *J. Phys. Chem.* **1995**, *103*, 869–875.
- [35] E. Moreno, D. Erni, C. Hafner, R. Vahldieck, *J. Opt. Soc. Am. A* **2002**, *19*, 101–111.
- [36] Y. C. Martin, H. F. Hamann, H. K. Wickramasinghe, *J. Appl. Phys.* **2001**, *89*, 5774–5778.
- [37] E. J. Zeman, G. C. Scahtz, *J. Phys. Chem.* **1987**, *91*, 634–643.
- [38] E. Hao, G. C. Scahtz, *J. Chem. Phys.* **2004**, *120*, 357–366.
- [39] M. Micic, N. Klymyshyn, Y. D. Suh, P. H. Lu, *J. Phys. Chem. B* **2003**, *107*, 1574–1584.
- [40] I. Notingher, A. Elfick, *J. Phys. Chem. B* **2005**, *109*, 15699–15706.
- [41] F. J. Garcia-Vidal, J. M. Pitarke, J. B. Pendry, *Phys. Rev. B* **1998**, *58*, 6783–6786.
- [42] W. A. Murray, W. L. Barnes, *Adv. Mater.* **2007**, *19*, 3771–3782.
- [43] K. L. Kelly, E. Coronado, L. L. Zhao, G. C. Scahtz, *J. Phys. Chem. B* **2003**, *107*, 668–677.
- [44] J. A. Creighton, C. G. Blatchford, M. G. Albrecht, *J. Chem. Soc. Faraday Trans. II* **1979**, *75*, 790–797.
- [45] C. G. Blatchford, J. R. Campbell, J. A. Creighton, *Surf. Sci.* **1982**, *120*, 435–455.
- [46] D. J. Maxwell, S. R. Emory, S. M. Nie, *Chem. Mater.* **2001**, *13*, 1082–1088.
- [47] M. Michaels, M. Nirmal, L. E. Brus, *J. Am. Chem. Soc.* **1999**, *121*, 9932–9939.
- [48] C. D. Keating, K. M. Kovalski, M. J. Natan, *J. Phys. Chem. B* **1998**, *102*, 9404–9413.
- [49] M. Moskovits, *J. Raman Spectrosc.* **2005**, *36*, 485.
- [50] H. X. Xu, M. J. Kall, *Chem. Phys. Chem.* **2003**, *4*, 1001–1005.
- [51] Z. Wang, S. Pan, T. D. Krauss, H. Du, L. J. Rothberg, *Proc. Natl. Acad. Sci. USA* **2003**, *100*, 8638–8643.
- [52] J. A. Dieringer, R. B. Lettan, II, K. A. Scheidt, R. P. Van Duyne, *J. Am. Chem. Soc.* **2007**, *129*, 16249–16256.
- [53] S. Nie, S. R. Emory, *Science* **1997**, *275*, 1102–1106.
- [54] A. M. Michaels, J. Jiang, L. Brus, *J. Phys. Chem. B* **2000**, *104*, 11965–11971.
- [55] P. C. Anderson, M. L. Jacobson, K. L. Rowlen, *J. Phys. Chem. B* **2004**, *108*, 2148–2153.
- [56] K. F. Domke, D. Zhang, B. Pettinger, *J. Phys. Chem. C* **2007**, *111*, 8611.
- [57] S. R. Emory, R. A. Jensen, T. Wenda, M. Han, S. Nie, *Faraday Discuss.* **2006**, *132*, 249–259.
- [58] S. K. Ghosh, T. Pal, *Chem. Rev.* **2007**, *107*, 4797–4862.
- [59] E. Hutter, J. H. Fendler, *Adv. Mater.* **2004**, *16*, 1685–1706.
- [60] A. M. Swartzberg, C. D. Grant, A. Wolcott, C. E. Talley, T. R. Huser, R. Bogomolni, J. Z. Zhang, *J. Phys. Chem. B* **2004**, *108*, 19191–19197.
- [61] J. M. McLellana, A. Siekkinena, J. Chena, Y. Xia, *Chem. Phys. Lett.* **2006**, *427*, 122–126.
- [62] G. H. Gu, J. Kim, L. Kim, J. S. Suh, *J. Phys. Chem. C* **2007**, *111*, 7906–7909.
- [63] J. Zhang, X. Li, X. Sun, Y. Li, *J. Phys. Chem. B* **2005**, *109*, 12544–12548.
- [64] N. R. Jana, T. Pal, *Adv. Mater.* **2007**, *19*, 1761–1765.
- [65] L. J. Sherry, R. Jin, C. A. Mirkin, G. C. Scahtz, R. P. Van Duyne, *Nano Lett.* **2006**, *6*, 2060–2065.
- [66] J. M. McLellan, A. Siekkinen, J. Chen, Y. Xia, *Chem. Phys. Lett.* **2006**, *427*, 122–126.
- [67] D. P. Fromm, A. Sundaramurthy, P. J. Schuck, G. S. Kino, W. E. Moerner, *Nano Lett.* **2004**, *4*, 957–961.
- [68] P. J. Schuck, D. P. Fromm, A. Sundaramurthy, G. S. Kino, W. E. Moerner, *Phys. Rev. Lett.* **2005**, *94*, 017402.
- [69] A. Sundaramurthy, K. B. Crozier, G. S. Kino, D. P. Fromm, P. J. Schuck, W. E. Moerner, *Phys. Rev. B* **2005**, *72*, 165409. 1–6.
- [70] R. Jin, Y. Cao, C. A. Mirkin, K. L. Kelly, G. C. Scahtz, J. G. Zheng, *Science* **2001**, *294*, 1901–1903.
- [71] Y. Sun, B. Mayers, Y. Xia, *Nano Lett.* **2003**, *3*, 675–679.
- [72] G. S. Metraux, C. A. Mirkin, *Adv. Mater.* **2005**, *17*, 412–414.
- [73] R. Jin, Y. C. Cao, E. Hao, G. Metraux, G. C. Scahtz, C. A. Mirkin, *Nature* **2003**, *425*, 487–490.
- [74] C. Xue, Z. Li, C. A. Mirkin, *Small* **2005**, *1*, 513–516.
- [75] J. E. Millstone, S. Park, K. L. Shuford, L. Qin, G. C. Scahtz, C. A. Mirkin, *J. Am. Chem. Soc.* **2005**, *127*, 5312–5313.
- [76] F. Kim, S. Connor, H. Song, T. Kuykendall, P. Yang, *Angew. Chem, Int. Ed.* **2004**, *43*, 3673–3677.
- [77] C. Li, W. Cai, Y. Li, J. Hu, P. Liu, *J. Phys. Chem. B* **2006**, *110*, 1546–1552.
- [78] J. S. Shumaker-Parry, H. Rochholz, M. Kreiter, *Adv. Mater.* **2005**, *17*, 2131–2134.
- [79] B. J. Wiley, Y. Chen, J. M. McLellan, Y. Xiong, Z. Li, D. Ginger, Y. Xia, *Nano Lett.* **2007**, *7*, 1032–1036.
- [80] C. J. Murphy, N. R. Jana, *Adv. Mater.* **2002**, *14*, 80–82.
- [81] J. M. McLellan, Z.-Y. Li, A. R. Siekkinen, Y. Xia, *Nano Lett.* **2007**, *7*, 1013–1017.
- [82] N. R. Jana, *Angew. Chem. Int. Ed.* **2004**, *43*, 1536–1540.
- [83] C. L. Nehl, H. Liao, J. H. Hafner, *Nano Lett.* **2006**, *6*, 683–688.
- [84] F. Hao, C. L. Nehl, J. H. Hafner, P. Nordlander, *Nano Lett.* **2007**, *7*, 729–732.
- [85] B. J. Kennedy, S. Spaeth, M. Dickey, K. T. Carron, *J. Phys. Chem. B.* **1999**, *103*, 3640–3646.
- [86] J. J. Storhoff, R. Elghanian, R. C. Mucic, C. A. Mirkin, R. L. Letsinger, *J. Am. Chem. Soc.* **1998**, *120*, 1959–1964.
- [87] P. K. Jain, W. Qian, M. A. El-Sayed, *J. Phys. Chem. B* **2006**, *110*, 136–142.
- [88] J. J. Storhoff, A. A. Lazarides, R. C. Mucic, C. A. Mirkin, R. L. Letsinger, G. C. Scahtz, *J. Am. Chem. Soc.* **2000**, *122*, 4640–4650.
- [89] C. Jiang, S. Markutsya, V. V. Tsukruk, *Langmuir* **2004**, *20*, 882–890.
- [90] J. A. Dieringer, A. D. McFarland, N. C. Shah, D. A. Stuart, A. V. Whitney, C. R. Yonzon, M. A. Young, X. Zhang, R. P. Van Duyne, *Faraday Discuss.* **2006**, *132*, 9–26.
- [91] A. V. Whitney, J. W. Elam, S. Zou, A. V. Zinovev, P. C. Stair, G. C. Scahtz, R. P. Van Duyne, *J. Phys. Chem. B* **2005**, *109*, 20522–20528.
- [92] B. Pettinger, K. F. Domke, D. Zhang, R. Schuster, G. Ertl, *Phys. Rev. B* **2007**, *76*, 113409.
- [93] W. Rechberger, A. Hohenau, A. Leitner, J. R. Krenn, B. Lamprecht, F. R. Aussenegg, *Opt. Commun.* **2003**, *220*, 137–141.
- [94] B. Lamprecht, G. Schider, R. T. Lechner, H. Dittlbacher, J. R. Krenn, A. Leitner, F. R. Aussenegg, *Phys. Rev. Lett.* **2000**, *84*, 4721–4724.
- [95] M. Salerno, N. Felidj, J. R. Krenn, A. Leitner, F. R. Aussenegg, J. C. Weeber, *Phys. Rev. B* **2001**, *63*, 165422.
- [96] J. R. Krenn, A. Dereux, J. C. Weeber, E. Bourillot, Y. Lacroute, J. P. Gouddonnet, G. Schider, W. Gotschy, A. Leitner, F. R. Aussenegg, C. Girard, *Phys. Rev. Lett.* **1999**, *82*, 2590–2593.
- [97] K. H. Su, Q.-H. Wei, X. Zhang, J. J. Mock, D. R. Smith, S. Schultz, *Nano Lett.* **2003**, *3*, 1087–1090.
- [98] L. Gunnarsson, T. Rindzevicius, J. Prikulis, B. Kasemo, M. Kall, S. Zou, G. C. Scahtz, *J. Phys. Chem. B* **2005**, *109*, 1079–1087.
- [99] P. K. Jain, W. Huang, M. A. El-Sayed, *Nano Lett.* **2007**, *7*, 2080–2088.
- [100] L. C. Brousseau, III, J. P. Novak, S. M. Marinakos, D. L. Feldheim, *Adv. Mater.* **1999**, *11*, 447–449.
- [101] J. G. Worden, A. W. Shaffer, Q. Huo, *Chem. Commun.* **2004**, 518–519.

- [102] A. W. Shaffer, J. G. Worden, Q. Huo, *Langmuir* **2004**, *20*, 8343–8351.
- [103] J. G. Worden, Q. Dai, A. W. Shaffer, Q. Huo, *Chem. Mater.* **2004**, *16*, 3746–3755.
- [104] K.-M. Sung, D. W. Mosley, B. R. Peelle, S. Zhang, J. M. Jacobson, *J. Am. Chem. Soc.* **2004**, *126*, 5064–5065.
- [105] S. T. Wang, J. Yan, L. Chen, *Mater. Lett.* **2005**, *59*, 1387–1390.
- [106] L. R. Hirsch, A. M. Gobin, A. R. Lowery, F. Tam, R. A. Drezek, N. Halas, J. L. West, *Anal. Biomed. Eng.* **2006**, *34*, 15–22.
- [107] E. Prodan, P. Nordlander, *J. Chem. Phys.* **2004**, *120*, 5444–5454.
- [108] J. B. Jackson, N. J. Halas, *J. Phys. Chem. B* **2001**, *105*, 2743.
- [109] S. J. Oldenburg, J. B. Jackson, S. L. Westcott, N. J. Halas, *Appl. Phys. Lett.* **1999**, *75*, 2897–2899.
- [110] E. Prodan, C. Radloff, N. Halas, P. Nordlander, *Science* **2003**, *302*, 419–422.
- [111] H. S. Zhou, I. Honma, H. Komiyama, *Phys. Rev. B* **1994**, *50*, 12052–12056.
- [112] S. J. Oldenburg, R. D. Averitt, S. L. Westcott, N. J. Halas, *Chem. Phys. Lett.* **1998**, *28*, 243–247.
- [113] P. Nordlander, C. Oubre, E. Prodan, K. Li, M. I. Stockman, *Nano Lett.* **2004**, *4*, 899–903.
- [114] P. Nordlander, E. Prodan, *Nano Lett.* **2004**, *4*, 2209–2213.
- [115] S. J. Oldenburg, S. L. Westcott, R. D. Averitt, N. J. Halas, *J. Chem. Phys.* **1999**, *111*, 4729–4735.
- [116] R. A. Alvarez-Puebla, D. J. Ross, G.-A. Nazri, R. F. Aroca, *Langmuir* **2005**, *21*, 10504–10508.
- [117] J. B. Jackson, N. J. Halas, *Proc. Natl. Acad. Sci. USA* **2004**, *101*, 17930–17935.
- [118] F. A. Jolesz, K. Hynynen, *Cancer J.* **2002**, *S1*, 100–112.
- [119] P. Mulvaney, M. Giersig, A. Henglein, *J. Phys. Chem.* **1993**, *97*, 7061–7064.
- [120] L. Rivas, S. Sanchez-Cortes, J. V. Garcia-Ramos, G. Morcillo, *Langmuir* **2006**, *16*, 9722–9728.
- [121] I. Srnová-Sýllofová, F. Lednický, A. Gemperlova, *Langmuir* **2000**, *16*, 9928–9935.
- [122] G. S. Métraux, Y. C. Cao, R. Jin, C. A. Mirkin, *Nano Lett.* **2003**, *3*, 519–522.
- [123] R. G. Sanedrin, D. G. Georganopoulou, S. Park, C. A. Mirkin, *Adv. Mater.* **2005**, *17*, 1027–1031.
- [124] S. E. Hunyadi, C. J. Murphy, *J. Mater. Chem.* **2006**, *16*, 3929–3935.
- [125] S. Pande, S. K. Ghosh, S. Praharaj, S. Panigrahi, S. Basu, S. Jana, A. Pal, T. Tsukuda, T. Pal, *J. Phys. Chem. C* **2007**, *111*, 10806–10813.
- [126] S. Guo, L. Wang, Y. Wang, Y. Fang, E. Wang, *Science* **2007**, *315*, 363–368.
- [127] L. M. Liz-Marzán, *Langmuir* **2007**, *22*, 32–41.
- [128] G. C. Papavassiliou, *Prog. Solid State Chem.* **1979**, *12*, 185–271.
- [129] S. W. Hans, Y. Kim, K. Kim, *J. Colloid Interface Sci.* **1998**, *208*, 272–278.
- [130] S. Link, Z. L. Wang, M. A. El-Sayed, *J. Phys. Chem. B* **1999**, *103*, 3529–3533.
- [131] M. P. Mallin, C. J. Murphy, *Nano Lett.* **2002**, *2*, 1235–1238.
- [132] K. Kim, K. L. Kim, S. J. Lee, *Chem. Phys. Lett.* **2005**, *403*, 77–82.
- [133] R. Gunawidjaja, S. Peleshanko, H. Ko, V. V. Tsukruk, *Adv. Mater.* **2008**, *20*, 1544–1549.
- [134] M. Quinten, A. Leitner, J. R. Krenn, F. R. Aussenegg, *Opt. Lett.* **1998**, *23*, 1331–1333.
- [135] S. A. Maier, M. L. Brongersma, P. G. Kik, S. Meltzer, A. A. G. Requicha, H. A. Atwater, *Adv. Mater.* **2001**, *13*, 1501–1505.
- [136] J. R. Krenn, A. Dereux, J. C. Weeber, E. Bourillot, Y. Lacroute, J. P. Goudonnet, G. Schider, W. Gotschy, A. Leitner, F. R. Aussenegg, C. Girard, *Phys. Rev. Lett.* **1999**, *82*, 2590–2593.
- [137] S. A. Maier, M. L. Brongersma, P. G. Kik, H. A. Atwater, *Phys. Rev. B* **2002**, *65*, 193408.
- [138] S. A. Maier, P. G. Kik, H. A. Atwater, *Appl. Phys. Lett.* **2002**, *81*, 1714–1716.
- [139] Q.-H. Wei, K.-H. Su, S. Durant, X. Zhang, *Nano Lett.* **2004**, *4*, 1067–1071.
- [140] R. de Waele, A. F. Koenderink, A. Polman, *Nano Lett.* **2007**, *7*, 2004–2008.
- [141] S. Zou, G. C. Schatz, *Chem. Phys. Lett.* **2005**, *403*, 62–67.
- [142] K. Li, M. I. Stockman, D. J. Bergman, *Phys. Rev. Lett.* **2003**, *91*, 227402.
- [143] J. R. Krenn, A. Dereux, J. C. Weeber, E. Bourillot, Y. Lacroute, J. P. Goudonnet, G. Schider, W. Gotschy, A. Leitner, F. R. Aussenegg, C. Girard, *Phys. Rev. Lett.* **1999**, *82*, 2590–2593.
- [144] S. A. Maier, P. G. Kik, H. A. Atwater, *Appl. Phys. Lett.* **2002**, *81*, 1714–1716.
- [145] Q.-H. Wei, K.-H. Su, S. Durant, X. Zhang, *Nano Lett.* **2004**, *4*, 1067–1071.
- [146] Z. Tang, N. A. Kotov, *Adv. Mater.* **2005**, *17*, 951–957.
- [147] J. Zeng, J. Huang, W. Lu, X. Wang, B. Wang, S. Zhang, J. Hou, *Adv. Mater.* **2007**, *19*, 2172–2176.
- [148] S. Lin, M. Li, E. Dujardin, C. Girard, S. Mann, *Adv. Mater.* **2005**, *17*, 2553–2559.
- [149] Y. Yang, S. Matsubara, M. Nogami, J. Shi, W. Huang, *Nanotechnology* **2006**, *17*, 2821–2827.
- [150] Y. Yang, J. Shi, T. Tanaka, M. Nogami, *Langmuir* **2007**, *23*, 12042–12047.
- [151] B. Nikoobakht, Z. L. Wang, M. A. El-Sayed, *J. Phys. Chem. B* **2000**, *104*, 8635–8640.
- [152] L. Qin, S. Park, L. Huang, C. A. Mirkin, *Science* **2005**, *309*, 113–115.
- [153] L. Qin, S. Zhou, C. Xue, A. Atkinson, G. C. Schatz, C. A. Mirkin, *Proc. Natl. Acad. Sci. USA* **2006**, *103*, 13300–13303.
- [154] L. Qin, M. J. Banholzer, J. E. Millstone, C. A. Mirkin, *Nano Lett.* **2007**, *7*, 3849–3853.
- [155] D. A. Genov, A. K. Sarychev, V. M. Shalaev, A. Wei, *Nano Lett.* **2004**, *4*, 153–158.
- [156] W. H. Binder, *Angew. Chem. Int. Ed.* **2005**, *44*, 5172–5175.
- [157] H. Duan, D. Wang, D. G. Kurth, H. Mohwald, *Angew. Chem, Int. Ed.* **2004**, *43*, 5639–5642.
- [158] J. Liao, L. Bernard, M. Langer, C. Schonenberger, M. Calame, *Adv. Mater.* **2006**, *18*, 2444–2447.
- [159] A. Wei, *Chem. Commun.* **2006**, 1581–1591.
- [160] C.-F. Chen, S.-D. Tzeng, H.-Y. Chen, K.-J. Lin, S. Gwo, *J. Am. Chem. Soc.* **2008**, *130*, 824–826.
- [161] T. Qiu, X. L. Wua, J. C. Shen, P. K. Chu, *Appl. Phys. Lett.* **2006**, *89*(13), 1914.
- [162] B. Kim, S. L. Tripp, A. Wei, *J. Am. Chem. Soc.* **2001**, *123*, 7955–7956.
- [163] A. Wei, B. Kim, B. Sadtler, S. L. Tripp, *Chem. Phys. Chem.* **2001**, *12*, 743–745.
- [164] L. M. Liz-Marzán, *Langmuir* **2006**, *22*, 32–41.
- [165] H. Wang, C. S. Levin, N. J. Halas, *J. Am. Chem. Soc.* **2005**, *127*, 14992–14993.
- [166] H. Wang, J. Kundu, N. J. Halas, *Angew. Chem, Int. Ed.* **2007**, *46*, 9040–9044.
- [167] G. Decher, *Science* **1997**, *277*, 1232–1237.
- [168] *Multilayer Thin Films*, (Eds.: G. Decher, J. B. Schlenoff), Wiley-VCH, Weinheim, Germany **2003**.
- [169] Y. Lvov, G. Decher, H. Möhwald, *Langmuir* **1993**, *9*, 481–486.
- [170] V. V. Tsukruk, V. N. Bliznyuk, D. W. Visser, A. L. Cambell, T. Bunning, W. W. Adams, *Macromolecules* **1997**, *30*, 6615–6625.
- [171] P. T. Hammond, *Adv. Mater.* **2004**, *16*, 1271–1293.
- [172] A. A. Mamedov, N. A. Kotov, *Langmuir* **2000**, *16*, 5530–5533.
- [173] L. Zhai, F. C. Cebeci, R. E. Cohen, M. F. Rubner, *Nano Lett.* **2004**, *4*, 1349–1353.
- [174] X. Shi, M. Shen, H. Möhwald, *Prog. Polym. Sci.* **2004**, *29*, 987–1019.
- [175] F. Caruso, *Adv. Mater.* **2001**, *13*, 11–22.

- [176] C. Jiang, S. Markutsya, Y. Pikus, V. V. Tsukruk, *Nat. Mater.* **2004**, *3*, 721–728.
- [177] C. Jiang, S. Markutsya, V. V. Tsukruk, *Adv. Mater.* **2004**, *16*, 157–161.
- [178] C. Jiang, S. Markutsya, H. Shulha, V. V. Tsukruk, *Adv. Mater.* **2005**, *17*, 1669–1673.
- [179] X. Hu, W. Cheng, T. Wang, Y. Wang, E. Wang, S. Dong, *J. Phys. Chem. B* **2005**, *109*, 19385–19389.
- [180] C. Lu, H. Moehwald, A. Fery, *J. Phys. Chem. C* **2007**, *111*, 10082–10087.
- [181] R. Gunawidjaja, C. Jiang, H. Ko, V. V. Tsukruk, *Adv. Mater.* **2006**, *18*, 2895–2899.
- [182] N. Malikova, I. Pastoriza-Santos, M. Schierhorn, N. A. Kotov, L. M. Liz-Marzan, *Langmuir* **2002**, *18*, 3694–3697.
- [183] G. Jiang, A. Baba, H. Ikarashi, R. Xu, J. Locklin, K. R. Kashif, K. Shinbo, K. Kato, F. Kaneko, R. Advincula, *J. Phys. Chem. C* **2007**, *111*, 18687–18694.
- [184] C. P. Collier, R. J. Saykally, J. J. Shiang, S. E. Henrichs, J. R. Heath, *Science* **1998**, *277*, 1978–1980.
- [185] S. Paul, C. Pearson, A. Molloy, M. A. Cousins, M. Green, S. Koliopoulou, P. Dimitrakis, P. Normand, D. Tsoukalas, M. C. Petty, *Nano Lett.* **2003**, *3*, 533–536.
- [186] K. L. Genson, J. Holzmuller, O. F. Villacencio, D. V. McGrath, D. Vaknin, V. V. Tsukruk, *J. Phys. Chem. B* **2005**, *109*, 20393–20402.
- [187] V. V. Tsukruk, V. N. Bliznyuk, *Prog. Polym. Sci.* **1997**, *22*, 1089–1132.
- [188] K. L. Genson, J. Holzmuller, C. Jiang, J. Xu, J. D. Gibson, E. R. Zubarev, V. V. Tsukruk, *Langmuir* **2006**, *22*, 7011–7015.
- [189] A. Tao, F. Kim, C. Hess, J. Goldberger, R. He, Y. Sun, Y. Xia, P. Yang, *Nano Lett.* **2003**, *3*, 1229–1233.
- [190] Y. Lu, G. L. Liu, L. P. Lee, *Nano Lett.* **2005**, *5*, 5–9.
- [191] A. Tao, P. Sinsersuksakul, P. Yang, *Nat. Nanotechnol.* **2007**, *2*, 435–440.
- [192] O. D. Velev, A. M. Lenhoff, *Curr. Opin. Colloid Interface Sci.* **2000**, *5*, 56–63.
- [193] J. C. Hulteen, R. P. Van Duyne, *J. Vac. Sci. Technol. A* **1995**, *13*, 1553–1558.
- [194] J. C. Hulteen, D. A. Treichel, M. T. Smith, M. L. Duval, T. R. Jensen, R. P. Van Duyne, *J. Phys. Chem. B* **1999**, *103*, 3854–3863.
- [195] C. L. Haynes, R. P. Van Duyne, *J. Phys. Chem. B* **2003**, *107*, 7426–7433.
- [196] A. D. McFarland, M. A. Young, J. A. Dieringer, R. P. Van Duyne, *J. Phys. Chem. B* **2005**, *109*, 11279–11285.
- [197] A. J. Haes, C. L. Haynes, A. D. McFarland, G. C. Schatz, R. P. Van Duyne, S. Zou, *MRS Bull.* **2005**, *30*, 368–375.
- [198] X. Zhang, C. R. Yonzon, R. P. Van Duyne, *J. Mater. Res.* **2006**, *21*, 1083–1092.
- [199] S. J. Lee, A. R. Morrill, M. Moskovits, *J. Am. Chem. Soc.* **2006**, *128*, 2200–2201.
- [200] M. Schierhorn, S. J. Lee, S. W. Boettcher, G. D. Stucky, M. Moskovits, *Adv. Mater.* **2006**, *18*, 2829–2832.
- [201] G. Duan, W. Cai, Y. Luo, Y. Li, Y. Lei, *Appl. Phys. Lett.* **2006**, *89*(18), 1918.
- [202] H.-H. Wang, C.-Y. Liu, S.-B. Wu, N.-W. Liu, C.-Y. Peng, T.-H. Chan, C.-F. Hsu, J.-K. Wang, Y.-L. Wang, *Adv. Mater.* **2006**, *18*, 491–495.
- [203] F. J. Garcia-Vidal, J. B. Pendry, *Phys. Rev. Lett.* **1996**, *77*, 1163–1166.
- [204] S. O. Kucheyev, J. R. Hayes, J. Biener, T. Huser, C. E. Talley, A. V. Hamza, *Appl. Phys. Lett.* **2006**, *89*, 053102.
- [205] L. H. Qian, X. Q. Yan, T. Fujita, A. Inoue, M. W. Chen, *Appl. Phys. Lett.* **2007**, *90*, 153120.
- [206] O. D. Velev, P. M. Tessier, A. M. Lenhoff, E. W. Kaler, *Nature* **1999**, *401*, 548.
- [207] O. D. Velev, E. W. Kaler, *Adv. Mater.* **2000**, *12*, 531–534.
- [208] P. M. Tessier, O. D. Velev, A. T. Kalambur, A. M. Lenhoff, J. F. Rabolt, E. W. Kaler, *Adv. Mater.* **2001**, *13*, 396–400.
- [209] P. M. Tessier, O. D. Velev, A. T. Kalambur, J. F. Rabolt, A. M. Lenhoff, E. W. Kaler, *J. Am. Chem. Soc.* **2000**, *122*, 9554–9555.
- [210] D. M. Kuncicky, S. D. Christesen, O. D. Velev, *Appl. Spectrosc.* **2005**, *59*, 401–409.
- [211] D. M. Kuncicky, B. G. Prevo, O. D. Velev, *J. Mater. Chem.* **2006**, *16*, 1207–1211.
- [212] S. Chan, S. Kwon, T. W. Koo, L. P. Lee, A. A. Berlin, *Adv. Mater.* **2003**, *15*, 1595–1598.
- [213] T. L. Williamson, X. Guo, A. Zukoski, A. Sood, D. J. Diaz, P. W. Bohn, *J. Phys. Chem. B* **2005**, *109*, 20186–20191.
- [214] M. Saito, M. Shibusaki, S. Nakamura, M. Miyagi, *Opt. Lett.* **1994**, *19*, 710–712.
- [215] K. H. A. Lau, S. Tan, K. Tamada, M. S. Sander, W. Knoll, *J. Phys. Chem. B* **2004**, *108*, 10812–10818.
- [216] H. Ko, V. V. Tsukruk, *Small*, in press.
- [217] A. Amezcua-Correa, J. Yang, C. E. Finlayson, A. C. Peacock, J. R. Hayes, P. J. A. Sazio, J. J. Baumberg, S. M. Howdle, *Adv. Funct. Mater.* **2007**, *17*, 2024–2030.
- [218] H. Yan, C. Gu, C. Yang, J. Liu, G. Jin, J. Zhang, L. Hou, Y. Yao, *Appl. Phys. Lett.* **2006**, *89*, 204101.
- [219] Y. Han, M. K. Oo, Y. Zhu, S. Sukhishvili, L. Xiao, M. S. Demohan, W. Jinc, H. Du, *Proc. SPIE* **2007**, *6767*, 67670G.
- [220] T. W. Ebbesen, H. J. Lezec, H. F. Ghaemi, T. Thio, P. A. Wolff, *Nature* **1998**, *391*, 667–669.
- [221] C. Genet, T. W. Ebbesen, *Nature* **2007**, *445*, 39–46.
- [222] A. G. Brolo, S. C. Kwok, M. G. Moffitt, R. Gordon, J. Riordon, K. L. Kavanagh, *J. Am. Chem. Soc.* **2005**, *127*, 14936–14941.
- [223] S. M. Williams, K. R. Rodriguez, S. Teeters-Kennedy, A. D. Stafford, S. R. Bishop, U. K. Lincoln, J. V. Coe, *J. Phys. Chem. B* **2004**, *108*, 11833–11837.
- [224] M. E. Stewart, C. R. Anderton, L. B. Thompson, J. Maria, S. K. Gray, J. A. Rogers, R. G. Nuzzo, *Chem. Rev.* **2008**, *108*, 494–521.
- [225] J. Dintinger, S. Klein, T. W. Ebbesen, *Adv. Mater.* **2006**, *18*, 1267–1270.
- [226] T. A. Kelf, Y. Sugawara, R. M. Cole, J. J. Baumberg, M. E. Abdelsalam, S. Cintra, S. Mahajan, A. E. Russell, P. N. Bartlett, *Phys. Rev. B* **2006**, *74*, 245415.
- [227] J. J. Baumberg, T. A. Kelf, Y. Sugawara, S. Cintra, M. E. Abdelsalam, P. N. Bartlett, A. E. Russell, *Nano Lett.* **2005**, *5*, 2262–2267.
- [228] E.-S. Kwak, J. Henzie, S.-H. Chang, S. K. Gray, G. C. Schatz, T. W. Odom, *Nano Lett.* **2005**, *5*, 1963–1967.
- [229] J. Henzie, M. H. Lee, T. W. Odom, *Nat. Nanotechnol.* **2007**, *2*, 549–554.
- [230] M. E. Stewart, N. H. Mack, V. Malyarchuk, J. A. N. T. Soares, T.-W. Lee, S. K. Gray, R. G. Nuzzo, J. A. Rogers, *Proc. Natl. Acad. Sci. USA* **2006**, *103*, 17143–17148.
- [231] A. G. Brolo, E. Arctander, R. Gordon, B. Leathem, K. L. Kavanagh, *Nano Lett.* **2004**, *4*, 2015–2018.
- [232] T. H. Reilly, III, S.-H. Chang, J. D. Corbman, G. C. Schatz, K. L. Rowlen, *J. Phys. Chem. C* **2007**, *111*, 1689–1694.
- [233] A. Lesuffleur, L. K. S. Kumar, A. G. Brolo, K. L. Kavanagh, R. Gordon, *J. Phys. Chem. C* **2007**, *111*, 2347–2350.
- [234] S. P. Mulvaney, C. D. Keating, *Anal. Chem.* **2000**, *72*, 145R–157R.
- [235] L. A. Lyon, C. D. Keating, A. F. Fox, B. E. Baker, L. He, S. R. Nicewarner, S. P. Mulvaney, M. J. Natan, *Anal. Chem.* **1998**, *70*, 341R–361R.
- [236] D. S. Grubisha, R. J. Lipert, H. Y. Park, J. Driskell, M. D. Porter, *Anal. Chem.* **2003**, *75*, 5936–5943.
- [237] X. Zhang, M. A. Young, O. Lyandres, R. P. Van Duyne, *J. Am. Chem. Soc.* **2005**, *127*, 4484–4489.
- [238] R. M. Jarvis, A. Brooker, R. Goodacre, *Anal. Chem.* **2004**, *76*, 5198–5202.

- [239] K. E. Shafer-Peltier, C. L. Haynes, M. R. Gluksberg, R. P. Van Duyne, *J. Am. Chem. Soc.* **2003**, *125*, 588–593.
- [240] M. Culha, D. Stokes, L. R. Allain, T. Vo-Dinh, *Anal. Chem.* **2003**, *75*, 6196–6201.
- [241] S. Shanmukh, L. Jones, J. Driskell, Y. Zhao, R. Dluhy, R. A. Tripp, *Nano Lett.* **2006**, *6*, 2630–2636.
- [242] D. A. Stuart, J. M. Yuen, N. Shah, O. Lyandres, C. R. Yonzon, M. R. Gluksberg, J. T. Walsh, R. P. Van Duyne, *Anal. Chem.* **2006**, *78*, 7211–7215.
- [243] X. Qian, X.-H. Peng, D. O. Ansari, Q. Yin-Geon, G. Z. Chen, D. M. Shin, L. Yang, A. N. Young, M. D. Wang, S. Nie, *Nat. Biotechnol.* **2008**, *26*, 83–90.
- [244] W. E. Doering, M. E. Piotti, M. J. Natan, R. G. Freeman, *Adv. Mater.* **2007**, *19*, 3100–3108.
- [245] D. S. Moore, *Rev. Sci. Instrum.* **2004**, *75*, 2499–2512.
- [246] K. Kneipp, Y. Wang, R. R. Dasari, M. S. Feld, B. D. Gilbert, J. Janni, I. Steinfeld, *Spectrochim. Acta A* **1995**, *51*, 2171–2715.
- [247] S. J. Toal, W. C. Trogler, *J. Mater. Chem.* **2006**, *16*, 2871–2883.
- [248] K. M. Spencer, J. M. Sylvia, J. A. Janni, J. D. Klein, *Proc. SPIE* **1999**, *3710*, 373–379.
- [249] R. J. Dijkstra, W. J. J. M. Scheenen, N. Dam, E. W. Roubos, J. J. ter Meulen, *J. Neurosci. Methods* **2007**, *159*, 43–50.
- [250] S. Kundu, M. Mandal, S. K. Ghosh, T. Pal, *J. Colloid Interface Sci.* **2004**, *272*, 134.
- [251] W.-W. Zhang, X.-M. Ren, H.-F. Li, J.-L. Xie, C.-S. Lu, Y. Zou, Z.-P. Ni, Q.-J. Meng, *J. Colloid Interface Sci.* **2003**, *268*, 173–180.
- [252] C. S. Levin, B. G. Janesko, R. Bardhan, G. E. Scuseria, J. D. Hartgerink, N. J. Halas, *Nano Lett.* **2006**, *6*, 2617–2621.
- [253] S. Webster, D. N. Batchelder, D. A. Smith, *Appl. Phys. Lett.* **1998**, *72*, 1478–1480.
- [254] C. Jiang, W. Y. Lio, V. V. Tsukruk, *Phys. Rev. Lett.* **2005**, *95*, 115503.
- [255] D. H. Kim, K. H. A. Lau, J. W. F. Robertson, O.-J. Lee, U. Jeong, J. I. Lee, C. J. Hawker, T. P. Russell, J. K. Kim, W. Knoll, *Adv. Mater.* **2005**, *17*, 2442–2446.
- [256] M. Maldovan, E. L. Thomas, *Nat. Mater.* **2004**, *3*, 593–600.
- [257] J. Biener, G. W. Nyce, A. M. Hodge, M. M. Biener, A. V. Hamza, S. A. Maier, *Adv. Mater.* **2008**, *6*, 1211–1217.
- [258] M. R. Bockstaller, R. A. Mickiewicz, E. L. Thomas, *Adv. Mater.* **2005**, *17*, 1331–1349.
- [259] S. V. Gaponenko, *Phys. Rev. B* **2002**, *65*, 140303.
- [260] J. Hiller, J. D. Mendelsohn, M. F. Rubner, *Nat. Mater.* **2002**, *1*, 59–63.
- [261] C. Jiang, V. V. Tsukruk, *Adv. Mater.* **2006**, *18*, 829–840.
- [262] I. Luzinov, S. Minko, V. V. Tsukruk, *Prog. Polym. Sci.* **2004**, *29*, 635–698.
- [263] J. Park, L. D. Fouche, P. T. Hammond, *Adv. Mater.* **2005**, *17*, 2575–2579.
- [264] D. Li, Y. Wang, Y. Xia, *Adv. Mater.* **2004**, *16*, 361–366.
- [265] Y. Dzenis, *Science* **2004**, *304*, 1917–1919.
- [266] R. Vendamme, S.-Y. Onoue, A. Nakao, T. Kunitake, *Nat. Mater.* **2006**, *5*, 494–501.

Received: March 6, 2008